REPORT DOCUMENTATION PAGE

AFRL-SR-AR-TR-04-

0219

1. REPORT DATE (DD-MM-YYYY)	2. REPORT TYPE	3. DATES COVERED (From - To)
4/12/2004	Final Report	12/01/2000 - 02/29/2004

4. TITLE AND SUBTITLE
Femtosecond Photonics: Fundamental Phenomena and Advanced Devices

5a. CONTRACT NUMBER
F49620-01-1-0084

5b. GRANT NUMBER

5c. PROGRAM ELEMENT NUMBER

6. AUTHOR(S)
Prof. Erich Ippen, Prof. Hermann Haus, Prof. James Fujimoto, Prof. Franz Kaertner

5d. PROJECT NUMBER

5e. TASK NUMBER

5f. WORK UNIT NUMBER

7. PERFORMING ORGANIZATION NAME(S) AND ADDRESS(ES)

Research Lab. of Electronics
Mass Inst. Of Technology
77 Mass Avenue
Cambridge, MA 02139

8. PERFORMING ORGANIZATION REPORT NUMBER

9. SPONSORING / MONITORING AGENCY NAME(S) AND ADDRESS(ES)
A.F. Office of Scientific Research
4015 Wilson Blvd. Rm. 713
Arlington, VA 22203-1954

10. SPONSOR/MONITOR'S ACRONYM(S)

11. SPONSOR/MONITOR'S REPORT NUMBER(S)

12. DISTRIBUTION / AVAILABILITY STATEMENT
Distribution Statement A: unlimited

13. SUPPLEMENTARY NOTES

14. ABSTRACT

Ultrashort pulse laser technology is an active field of research that has had a powerful impact in many areas of science. Applications of ultrafast technology range from biomedical optical imaging such as optical coherence tomography (OCT), to high-speed communications, investigation of ultrafast nonlinear process in semiconductor materials and devices, optical frequency metrology, the design of optical clocks, and micro-machining.

20040426 064

15. SUBJECT TERMS

16. SECURITY CLASSIFICATION OF:			17. LIMITATION OF ABSTRACT	18. NUMBER OF PAGES	19a. NAME OF RESPONSIBLE PERSON
a. REPORT	b. ABSTRACT	c. THIS PAGE			19b. TELEPHONE NUMBER (include area code)

FINAL REPORT 2004

Air Force Office of Scientific Research
Contract No. F49620-01-1-0084

FEMTOSECOND PHOTONICS: FUNDAMENTAL PHENOMENA AND ADVANCED DEVICES

Principal Investigators

Professor Erich P. Ippen
Professor Hermann A. Haus
Professor James G. Fujimoto
Professor Franz Kaertner

Address

The Research Laboratory of Electronics
Massachusetts Institute of Technology
77 Massachusetts Avenue
Cambridge, MA 02139

FINAL REPORT

Air Force Office of Scientific Research
Contract No. F49620-01-1-0084

Principal Investigators

Professor Erich P. Ippen
Professor Hermann A. Haus
Professor James G. Fujimoto
Professor Franz Kaertner

Objective of the Proposal

To perform the research necessary for the development of future ultrafast photonic technology.

Accomplishments

Over the three years of work under this contract we have made significant progress in the development of new ultrashort pulse lasers and ultrafast techniques, in the application of ultrafast optics to novel materials and material structures, and to the development of microphotonic devices. Some of these key advances are summarized in sections entitled:

A. Ultrashort Pulse Laser Technology
B. Multi-pass Femtosecond Laser Cavitie
C. High-repetition-rate Semiconductor, Microchip and Fiber Lasers
D. Studies of Ultrafast Phenomena in Materials and Devices
E. Femtosecond Nonlinear Material Processing

A list of publications acknowledging this contract is appended at the end.

Ultrashort-pulse Laser Technology

Ultrashort pulse laser technology is an active field of research that has had a powerful impact in many areas of science. Applications of ultrafast technology range from biomedical optical imaging such as optical coherence tomography (OCT), to high-speed communications, investigation of ultrafast nonlinear process in semiconductor materials and devices, optical frequency metrology, the design of optical clocks, and micro-machining.

Kerr-lens modelocking (KLM) has been the most successful technique for the generation of ultrashort pulses. The performance of these laser systems depends critically upon the ability to compensate dispersion over broad bandwidth ranges. Over the last three years our group has developed several new ultrashort pulsed KLM lasers based on the use of double-chirped mirrors (DCMs) for dispersion management, covering the wavelength range from 600 nm to 1500 nm. This range is of particular interest because it includes the first three telecommunication windows as well as biological chromophores such as the hemoglobin and water absorption bands, making our sources useful not only for the investigation of fibers and photonic devices but also for biomedical imaging. One important direction has been the development of ultrabroadband sources capable of producing octave-spanning spectra. These sources enable direct optical frequency referencing using the $1f - 2f$ technique [1] which is critical for frequency metrology and optical clock design. Another direction has been the use of multiple-pass cavities to scale laser pulse energies, enable low threshold laser operation, and compact cavity design. High pulse energy lasers are used for micro-machining photonic devices. High energies also improve the efficiency of nonlinear processes such as frequency generation, frequency broadening in nonlinear fibers, and pump probe measurements.

In the design of ultrashort sources one of the most important considerations is proper dispersion management. The use of prism compressors (prism pairs) has been the most popular technique for intracavity dispersion compensation and has been able to provide sub-10 fs pulses [2], but has not been able to break the 8 fs mark due to unbalanced higher order dispersion. To generate even shorter optical pulses a broader bandwidth dispersion compensation approach is required. This technology was invented only a few years ago in the form of chirped and double-chirped mirrors.

Singly chirped mirrors, shown in Figure 1(b), were designed by Szipöcs et al. [3, 4] based on the Bragg mirror structure shown in Figure 1(a). They consisted of dielectric layers of increasing thickness that offered both high reflectivity at a range of wavelengths and different penetration depths to the different wavelength components. In particular, they helped compensate dispersion by making the longer wavelengths travel a greater distance than the shorter wavelengths. However, because impedance matching between layers was not taken into account, they suffered from multiple reflections and wavelength dependent oscillations in the dispersion compensation.

Further investigation and an exact coupled-mode theory for multilayer devices [5] led to the recent invention of "double-chirped mirrors" (DCMs) [6, 7], shown in Figure 1(c). In DCMs better impedance matching by chirping not only the Bragg wavelength but also the thickness of the high index material, helped smooth out the undesired oscillations and led to much better performance. Our group has applied DCM technology to many solid state materials to achieve record pulse duration and bandwidth performance.

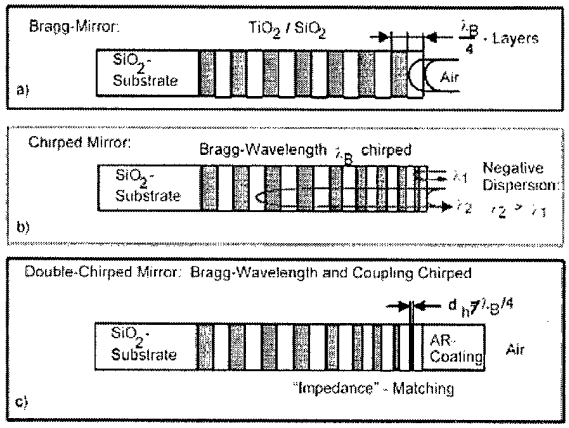

Figure 1. Schematic of the layer sequence for various dielectric mirrors: (a) standard quarter wave Bragg mirror, (b) simple chirped mirror, (c) double chirped mirror (DCM).

Ultrabroadband Ti:sapphire laser

Dispersion management techniques using DCMs can be applied to a wide range of solid state materials and wavelength ranges. Using this new technology, our group has recently demonstrated the generation of 5 fs pulses and spectral bandwidths greater than one octave directly from a Ti:sapphire laser [8]. These are the shortest pulses ever generated directly from a laser without any external compression. The schematic of our laser is shown in Figure 2. It has a 2.7 mm Ti:sapphire crystal placed in a double Z-fold cavity. A second focus is created between mirrors M4 and M5 where a 2.4 mm thick plate of BK7 is placed. This plate provides enhanced self phase modulation (SPM) and increases the laser bandwidth. Eight bounces on the DCM pairs and traveling through the prism pair per round trip compensates all of the intracavity dispersion and helps provide an octave of bandwidth extending from 600 to 1350 nm above the noise floor, as shown in Figure 3(b). The interferometric autocorrelation of the output pulses is shown in Figure 3(a). Using a phase retrieval algorithm to reconstruct the actual pulse shape from this data [9] we found these pulses to be 5 fs in duration (FWHM).

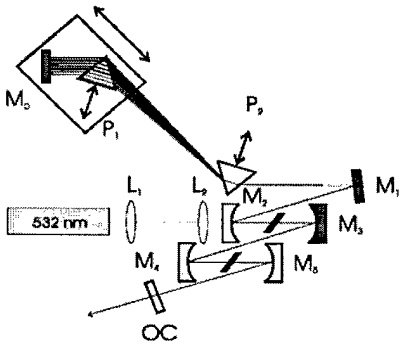

Figure 2. Schematic of the double Z-fold Ti:sapphire laser cavity that generates an octave bandwidth and 5 fs pulses. A 2.7 mm crystal is placed the first fold and a second focus in the second fold is used to increase the laser bandwidth via SPM. A prism pair and DCMs are used to compensate the intracavity dispersion. The laser is optically pumped by continuous wave light at 532 nm.

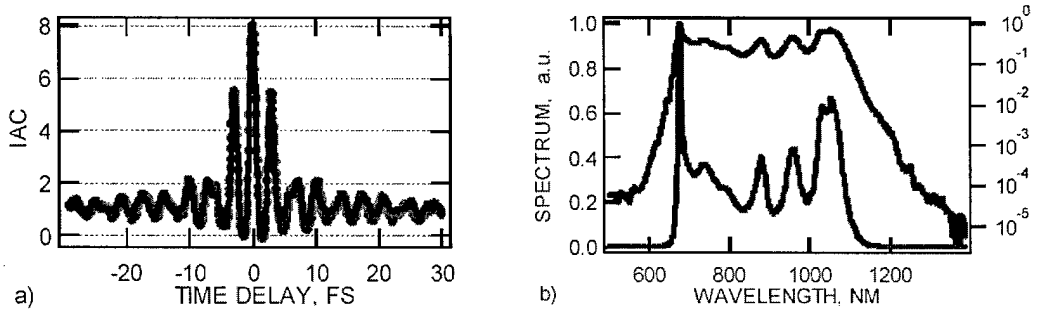

Figure 3. (a) Interferometric autocorrelation matches a fit corresponding to a 5 fs pulse. (b) Octave spanning spectrum of the Ti:sapphire laser plotted on linear and logarithmic scales

Complementary pair DCMs for ultrabroadband Ti:sapphire laser

The DCMs designed in our group provide very high reflectivity and well controlled dispersion compensation over 400 nm of bandwidth. These mirrors were used in our earlier work to generate pulses shorter than 5.4 fs at a repetition rate of 90 MHz, center wavelength of 800 nm, and with average output power of 200 mW, using a Kerr-lens mode-locked Ti:sapphire laser. Pulses this short correspond to an output bandwidth greater than 350 nm. Broad spectral bandwidths are important for biomedical optical imaging, ultrafast instrumentation, and other applications in femtosecond optics.

Ti:sapphire has a gain bandwidth extending from 600 nm to almost 1200 nm which, coupled with self phase modulation, should permit the generation of even shorter pulses with durations in the single cycle regime. However, this was not achieved in our earlier work because of the limited bandwidth over which each DCM could compensate the intracavity dispersion. It is possible to design the DCMs to provide larger bandwidths, but these extreme bandwidths also increase the oscillations in the group delay dispersion (GDD). To help overcome this bandwidth limitation we recently developed an analytic theory for the design of dispersion compensating mirrors and used it to fabricate specially matched double-chirped mirror pairs, for which the excess GDD oscillations of the first mirror are exactly out of phase with those of the second mirror. Such "complementary pair" DCMs can provide dispersion compensation over a much broader bandwidth than possible using a single mirror set. In particular, they can provide an octave of bandwidth [10], enabling the generation of unprecedented pulse durations.

Figure 4 shows the reflectivity and GDD curves of one of our complementary mirror pairs. These mirrors were designed to compensate intracavity dispersion up to sixth order and to transmit the pump light at 532 nm. They provide greater than 99.8% average reflectivity and cancel the GDD oscillations. These mirrors are high sensitive to design and fabrication parameters and fabrication requires careful process control.

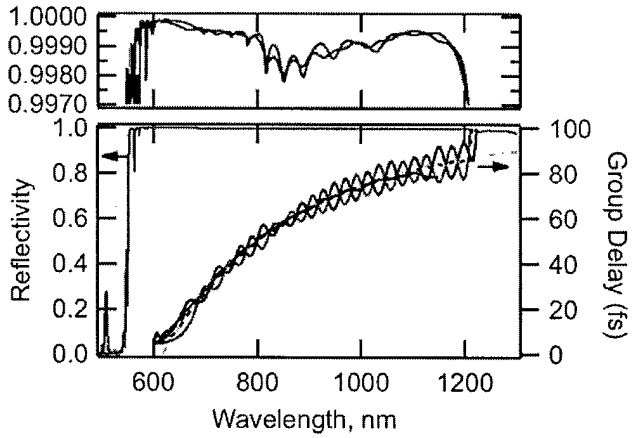

Figure 4. Group delay and reflectivity curves for the complimentary pair DCMs. The calculated reflectivity is shown by the solid curve with the scale to the left, and is shown in greater detail in the plot above. The group delay design goal for perfect dispersion compensation is shown by the dash-dotted line with the scale to the right. The group delay of each of the designed mirrors is shown with rippled solid curves and the measured group delay (the average of the two) is given by the solid curve between them. Note that the measured dispersion very closely follows the design goal over the 650-1100 nm range. The measurement was limited to 1100 nm because of the Si detector used.

Ultrabroadband prismless Ti:sapphire laser

Although prisms can be used together with DCMs to compensate intracavity dispersion, using a prism sequence prevents a compact laser layout and also increases the laser susceptibility to long term drifts because of beam variations in the prism pair. To avoid these drawbacks the laser must be built without intracavity prisms. Our most recent design of a prismless compact Ti:sapphire laser is shown in Figure 5. This laser has a 2 mm Ti:sapphire crystal placed in a standard Z-fold cavity and uses the novel complementary pair DCMs for all of the intracavity dispersion compensation. There are four bounces on the DCM pairs in the short arm and eight bounces on DCM pairs in the long arm per round trip. The additional BaF_2 plate in the short arm and BaF_2 wedge pair in the long arm permit fine adjustment of dispersion and to balance dispersion before and after pulse transit through the crystal. BaF_2 is chosen because it has the lowest third order dispersion compared to other fluorides and glasses that are transparent in the visible to near infrared region. This laser generated an average power output of 100 mW (for 3.7 W of pump power) at a repetition rate of 150 MHz.

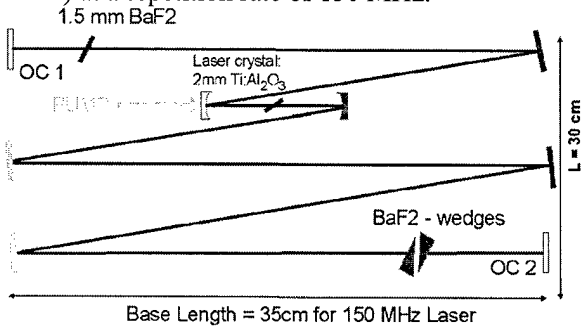

Figure 5. Schematic of the prismless Ti:sapphire laser Z-fold cavity using a 2 mm crystal and specially matched DCM pairs for all of the intracavity dispersion compensation. This laser produces an octave spanning spectrum.

The prismless design enables a compact system footprint of only (35x30 cm). The output spectrum is shown in Figure 6. Note that it is octave spanning at approximately 20 dB below the peak level. This enables this laser to be used for direct carrier envelope optical frequency referencing using the 1f – 2f technique [1]. Earlier studies showed that bandwidth limitations in this laser were not due to the mirrors but rather to roll-off in the output coupler. Increased output at the short and long wavelengths was possible using a new 2% broadband TiO_2/SiO_2 output coupler, OC1 in Figure 5. The other cavity end mirror, OC2, is a broadband silver mirror.

Obtaining well-shaped octave spanning spectra from these lasers is vital for future progress in frequency metrology, the design of optical clocks, and numerous other applications.

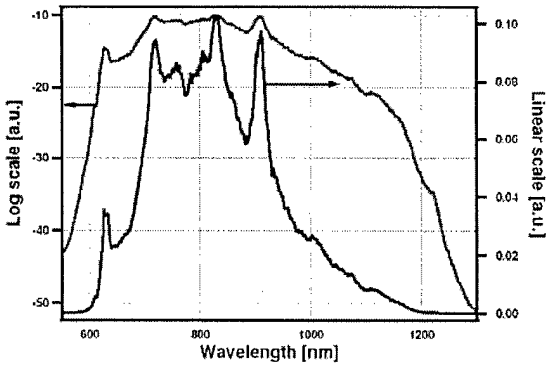

Figure 6. Octave spanning spectrum of the prismless Ti:sapphire laser plotted on linear and logarithmic scales. The octave of spectrum is obtained at approximately 20 dB below the peak level.

Ultralow-threshold, low-cost, broadband femtosecond laser technology

While solid-state femtosecond lasers provide outstanding performance, one of the major disadvantages of this technology is its high cost. The development of low-cost femtosecond broadband sources would enable a wide range of applications of femtosecond technology outside the research laboratory.

A standard KLM laser operating with a 5 W pump can produce output powers in the 500 mW range and bandwidths in excess of 150 nm [2]. However, the large size and high cost associated with these lasers has severely limited their widespread use. The large size is due to the standard use of intracavity prisms. The high cost, is the result of pump power requirements. In particular, typical ultrashort pulse sources require diode pumped solid-state lasers capable of providing powers in the 5 W range which typically cost $50,000. Pump laser costs increases with power, and pump sources generating several hundred mW are available for under $10,000.

We have recently demonstrated an ultra-low threshold modelocked Ti:sapphire laser with a record low modelocking threshold of only ~160 mW pump power [11]. This laser was built without DCMs, using all commercially available components so that it could be easily copied by other groups. Pulse durations as short as 14 fs with 100 nm bandwidths could be achieved. This laser can be built for a cost of 4-5x less than conventional laser sources. Using higher pump powers and DCMs pulse durations of ~10 fs and bandwidths of up to 160 nm could be achieved.

In order to demonstrate the feasibility of using these new lasers for practical applications outside the research laboratory, we recently developed a low-threshold modelocked Ti:sapphire laser suitable for clinical ultrahigh-resolution OCT imaging. The schematic of this laser is shown in Figure 7. It has a 2.05 mm Ti:sapphire crystal placed in a standard Z-fold cavity and uses DCMs to compensate all of the

intracavity dispersion. The entire cavity including pump source has been placed on a single lightweight breadboard measuring 19" by 45".

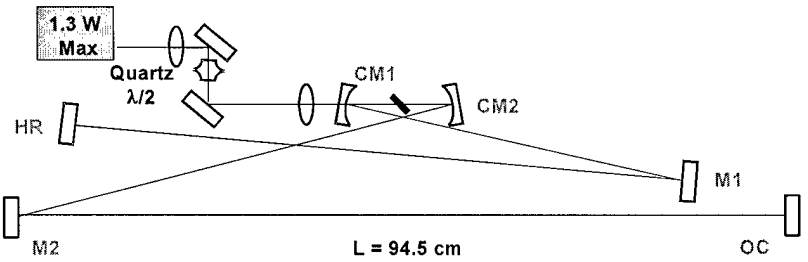

Figure 7. Schematic of the low-threshold prismless Ti:sapphire laser using a 2.05 mm crystal and double chirped mirrors for intracavity dispersion compensation and tuning.

This laser is pumped by a compact and low-cost 1.0 W pump laser. The Ti:sapphire laser generates 50 mW of average output power and 124 nm of bandwidth (FWHM). Ophthalmic OCT imaging was performed in the clinic of the New England Eye Center. Figure 8 shows an example comparing ultrahigh-resolution OCT imaging using the femtosecond light source versus standard resolution imaging using the commercial OCT instrument, the StratusOCT, from Carl Zeiss. Image resolutions can be improved from 10 μm to better than 3 μm. This yields a dramatic enhancement in image quality. Over 200 patients have been imaged to date.

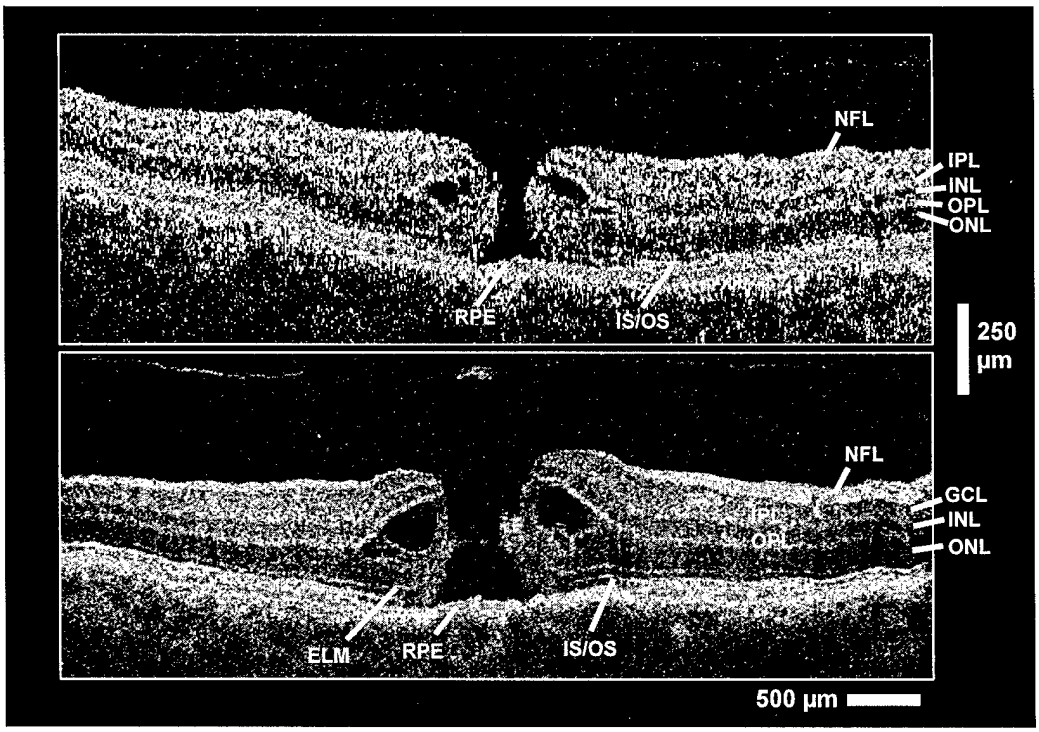

Figure 8. Comparison of standard resolution and ultrahigh resolution ophthalmic OCT image of a patient with a full thickness macular hole. Imaging was performed in the clinic of the New England Eye Center using our low threshold TiSapphire laser. Image resolution can be improved from 10 μm to better than 3 μm. Over 200 patients have been imaged to date.

Many disciplines will benefit from the availability of high-performance, low-cost femtosecond technology. Optical coherence tomography (OCT) is a rapidly emerging research area with applications in a wide range of clinical specialties. The availably of low-cost ultrabroadband laser sources will dramatically enhance image resolution as well as enabling spectroscopic imaging. Octave spanning femtosecond lasers can be carrier envelope stabilized, enabling a wide range of frequency metrology and optical clock applications. These sources will also enable the development of versatile and low-cost ultrafast measurement systems for spectroscopic characterization of materials and devices.

Ultrafast Cr^{4+}:YAG laser

Cr^{4+}:YAG is a promising laser crystal with broad emission from 1300 to 1600 nm. It provides access to one of the more interesting spectral ranges, centered around 1.5 um, which falls into the third telecommunications window. Previously, the shortest pulses available from a Cr^{4+}:YAG laser were 43 fs pulses [12], generated by a laser using a fused silica prism pair to compensate the group delay dispersion (GDD) of the Cr^{4+}:YAG crystal. In general, uncompensated higher order intracavity dispersion from the crystal, prisms, and mirrors limits the laser bandwidth and pulsewidth [13].

Double-chirped mirrors are a powerful technology for femtosecond pulse generation because they can compensate higher order intracavity dispersion. Using DCMs for dispersion management, our group recently demonstrated an all-solid-state, Kerr-lens modelocked Cr^{4+}:YAG laser producing ~20 fs pulses with 190 nm of bandwidth at 1450 nm. This is the shortest pulse duration ever generated by a Cr^{4+}:YAG laser [14]. An average output power of 200 to 400 mW (for 9 W of absorbed pump power) at a repetition rate of 110 MHz was achieved. A schematic of our Cr^{4+}:YAG laser is shown in Figure 9.

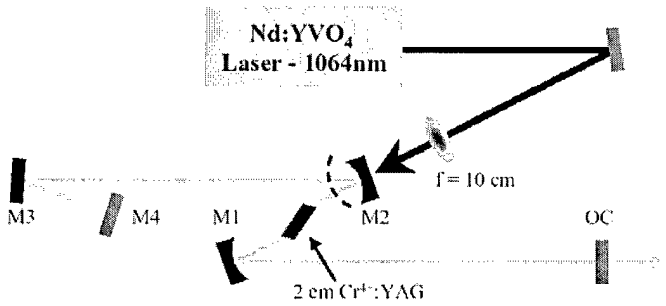

Figure 9. Schematic of the Cr^{4+}:YAG laser Z-fold cavity using a 2 cm crystal and DCMs for intracavity dispersion compensation. The laser is optically pumped by a Nd:YVO_4 laser emitting continuous wave light at 1064 nm.

The Cr^{4+}:YAG crystal is 2 cm long and is placed in a standard Z-fold cavity designed to maximize KLM while simultaneously compensating for astigmatism. Six round-trip bounces on the DCMs are used to compensate the GDD and the higher-order dispersion. The output spectrum of the laser and the interferometric autocorrelation are shown in Figures 10(a) and (b) respectively. In collaboration with Leslie Kolodziejski's group at MIT we have been designing, fabricating and testing novel ultrabroadband oxidized mirrors with integrated semiconductor saturable absorbers to facilitate self-starting and more stable operation.

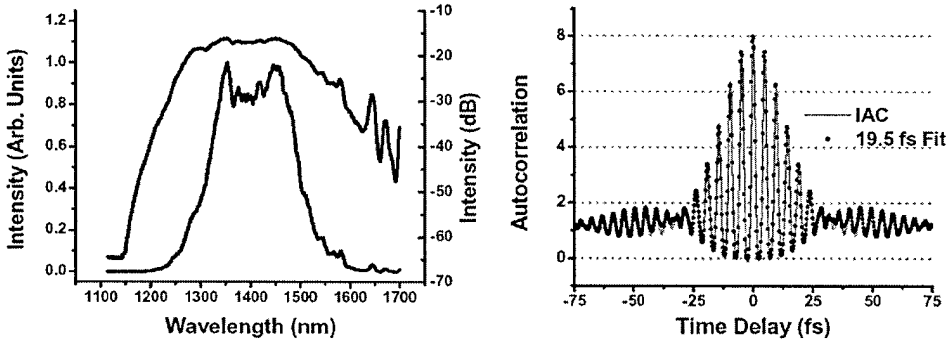

(a) (b)

Figure 10. a) Spectrum of the Cr^{4+}:YAG laser plotted on linear and logarithmic scales. The output has a spectral bandwidth of 190 nm (FWHM). b) Interferometric autocorrelation matches a fit corresponding to a 19.5 fs pulse. This is a record pulse duration.

Preliminary results [15] demonstrated stable self-starting operation with such a mirror albeit with slightly longer, 32 fs, pulse durations. We believe that this was due to peak-power-limiting by two-photon absorption in the small mirror surface. Very recent progress toward uniformly oxidized mirrors with larger areas promises to permit the generation of much shorter pulses. Figure 11 shows the structure of such a mirror as well as the ultrabroad bandwidth that is achievable with only 7 layer pairs.

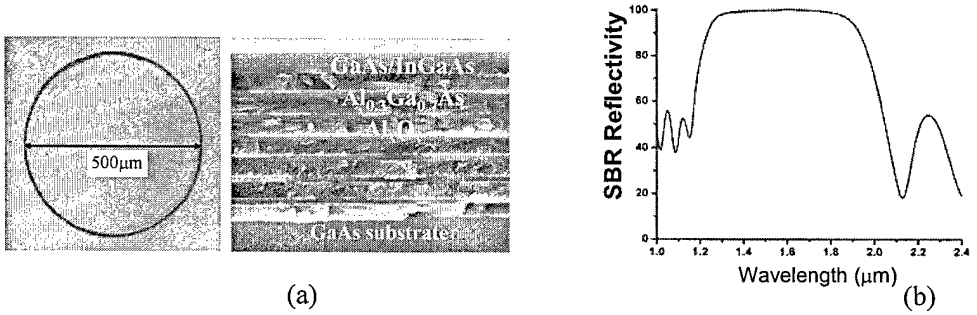

(a) (b)

Figure 11 a) Top and cross-section view of an oxidized GaAs/AlGaAs mirror stack, showing oxidation uniformity over more than a 500μm diameter. b) The ultrabroad reflectivity band of such a high-index contrast stack

High-performance Cr:forsterite lasers

Cr:forsterite is another very promising laser material. Like Cr^{4+}:YAG it provides access to an important spectral range, centered around 1.3 μm, which falls into the second telecommunications window. This wavelength range is also used in biomedical imaging because optical scattering is low and penetration of light into tissue is enhanced relative to shorter wavelengths. Dispersion compensation in the 1.3μm range is particularly difficult because many optical materials have their dispersion zeros in this range and therefore higher order dispersion becomes dominant. Therefore, DCMs provide one of the only methods for achieving broadband operation in this important laser system.

Our group recently demonstrated an all-solid-state, Kerr-lens modelocked Cr:forsterite laser using a combination of DCMs (except for the output coupler) along with a prism pair to tune the intracavity dispersion. A schematic of our Cr:forsterite laser is shown in Figure 13. The Cr:forsterite crystal is 5 mm long and is placed in a standard Z-fold cavity. Five bounces on the DCMs and traveling through the prism pair each round trip were used to compensate the intracavity dispersion. The prisms were made of PBH71

(SF58) glass which was chosen because its zero dispersion wavelength is 2 μm and therefore it has smaller residual third order dispersion relative to second order dispersion. The laser output spectrum and interferometric autocorrelation are shown in Figures 13(a) and (b) respectively. This laser produced 14 fs pulses with 250 nm bandwidth at 1.3 μm, which are the shortest pulses ever generated by a Cr:forsterite laser [16]. An average power output of 80 mW (for 6 W of pump power) at a repetition rate of 100 MHz was achieved.

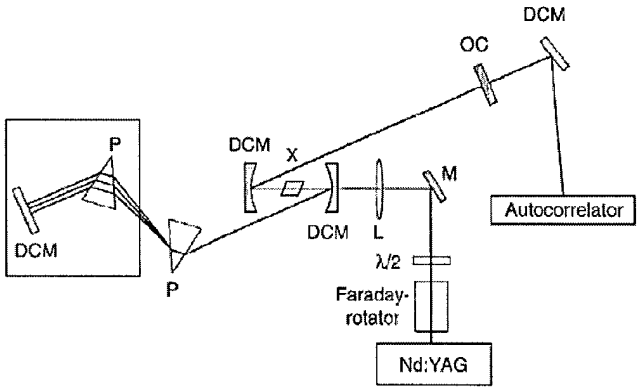

Figure 13. Schematic of the Cr:forsterite laser Z-fold cavity using a 5 mm crystal, DCMs for intracavity dispersion compensation and a prism pair to fine tune the dispersion.

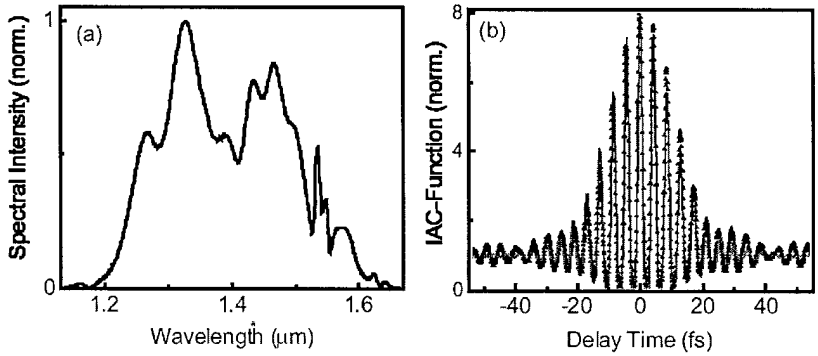

Figure 12. (a) Spectrum of the Cr:forsterite laser plotted on a linear scale. The output has a spectral bandwidth of 250 nm (FWHM). (b) Interferometric autocorrelation showing a pulse duration of 14 fs. This is a record pulse duration.

The development of a prismless Cr:forsterite laser would enable a compact and high-stability laser design. Recently, Thomann et al. demonstrated a Cr:forsterite ring laser using chirped mirrors that generates 30 fs pulses at a 420 MHz repetition rate with approximately 500 mW of average output power [17]. Dispersion compensation over a broad spectral range is challenging due to higher-order dispersion. The bandwidth was only 59 nm (FWHM), resulting in a relatively long pulse duration. Singly chirped mirrors such as those used by Thomann et al. are not capable of correcting for higher-order dispersion.

Our group has recently designed third generation DCMs which can compensate third-order as well as second-order dispersion. This technology should enable the construction of compact and high-stability Cr:forsterite lasers with broader spectra than previously reported [16]. Such a source would useful for direct optical frequency referencing using the 1f – 2f technique [1]. Applications would include optical frequency metrology, optical clock design, and the locking of this laser with other broadband sources such as Ti:sapphire lasers to provide extremely broad bandwidths. These lasers would also be useful for ultrahigh-resolution OCT imaging as well as high-resolution pump-probe characterization of materials and devices in the telecom wavelength range.

Multi-pass Femtosecond Laser Cavities

Herriott-type multi-pass cavities (MPC) enable the development of a wide range of new femtosecond laser designs. MPCs enable the laser pulse energy to be increased by extending the cavity path length and decreasing the repetition rate. MPCs also enable the development of very compact lasers while preserving standard repetition rates and pulse energies. In its simplest form, an MPC consists of a stable two-mirror resonator. A schematic is shown in Figure 14, where beam injection and extraction occur by use of notches. When the MPC parameters are properly adjusted, the incident beam injected with the correct offset and tilt, undergoes multiple bounces before exiting. The successive bounces of the beam viewed in a given reference plane (for example on one of the end mirrors) form an elliptical or circular spot pattern. Using appropriate design conditions, the MPC can leave the Gaussian beam q parameter invariant. This means that diffractive beam spreading effects are exactly cancelled as a result of the periodic focusing inside the cavity. First introduced by Herriott et al.[18,19], MPCs have long been used in many applications such as accurate optical loss measurements [18], stimulated Raman scattering [20,21], long-path absorption spectroscopy [22], and high-speed path-length scanning [23].

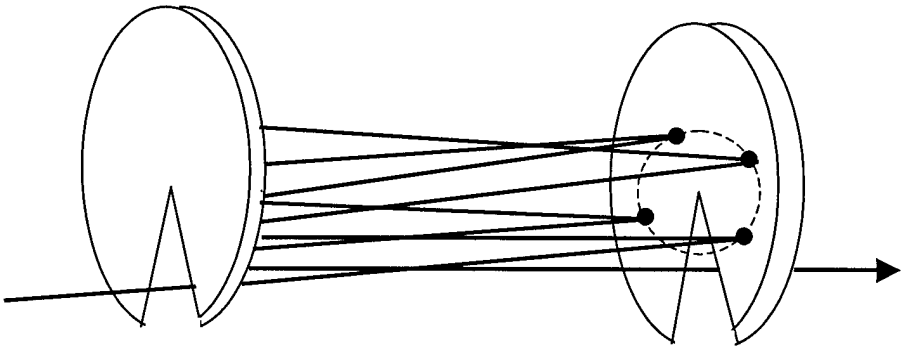

Figure 14. Schematic of a multi-pass cavity (MPC). With careful design, the q parameter of the beam is left invariant. MPCs can be used to increase pulse energy or reduce cavity size.

Previous studies have demonstrated improvements in laser pulse energy using low repetition rate femtosecond lasers created by extending the laser cavity with relaying imaging [24]. Recently high pulse energy, KLM femtosecond lasers using MPCs for extending the cavity length have been demonstrated [25,26]. Increasing the overall cavity path length lowers the pulse repetition rate while maintaining the same average output power and thereby increases the output pulse energy. Furthermore, since amplifiers or cavity dumpers are not required, the system design is simplified and the overall cost is significantly reduced. These laser sources are attractive in many applications such as pump-probe studies where high-energy pulses at reduced average powers obviate undesirable effects such as thermal loading.

Formulating general design rules for multi-pass cavities

Several issues need to be addressed in the practical design of MPCs for high-energy ultrafast lasers. In general, the cavity operating point is very important for Kerr lens modelocked operation and modelocking is only possible in a small subset of the cavity stability region. If the cavity repetition rate is increased by extending the length of a standard four-mirror cavity, the cavity operating point, including the stability region and spot sizes change dramatically. This makes re-establishing KLM operation very difficult. These problems are solved by keeping the q parameter invariant. In addition, even if the pulse energy changes as a result of using an MPC, keeping the same q parameter operating point is important if the laser is modelocked in the soliton pulse regime. In this case, the cavity dispersion is proportionally scaled up as the pulse energy is increased to enable the generation of pulses with approximately the same duration. For these reasons, maintaining the same q parameter is desirable. This is guaranteed if the MPC

is designed in such a way that the exiting beam has the same q parameter as the beam incident on the MPC. We refer to this as the "q preserving" configuration of the MPC.

Recently, we have developed general guidelines for the design of q-preserving MPCs which enable the design of a wide range of lasers [27]. Here, we will briefly review the general results of this analysis. In an MPC, a single round trip can be represented by a ray transfer matrix M_T

$$M_T = \begin{bmatrix} A & B \\ C & D \end{bmatrix}. \tag{1}$$

The stability requirement is similar to that of a 2-mirror resonator, and the elements A and D of M_T must satisfy the inequality

$$\left| \frac{A+D}{2} \right| \leq 1, \tag{2}$$

in order for the MPC to be stable. In this particular case, the matrix M_T^n that describes n roundtrips inside the MPC can be written in the form

$$M_T^n = \begin{bmatrix} \frac{A-D}{2}\frac{\sin n\theta}{\sin\theta} + \cos n\theta & B\frac{\sin n\theta}{\sin\theta} \\ C\frac{\sin n\theta}{\sin\theta} & \frac{D-A}{2}\frac{\sin n\theta}{\sin\theta} + \cos n\theta \end{bmatrix}. \tag{3}$$

Here, θ can be calculated from the relation

$$\cos\theta = \frac{A+D}{2}. \tag{4}$$

When the initial offset and the tilt of the incident beam are adjusted to obtain a circular spot pattern as the beam bounces between the mirrors, θ corresponds to the angular advance of the spot after one round trip. This is sketched in Figure 15.

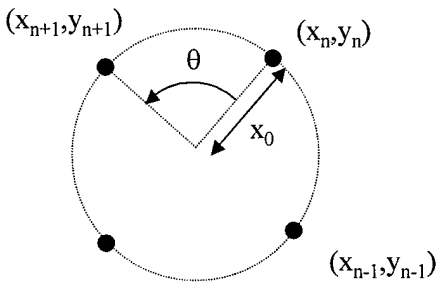

Figure 15. Spot-pattern formed on one of the mirrors of a multi-pass cavity. θ corresponds to the angular advance of the beam after each round trip.

If the MPC is q-preserving, the q parameter of the returning beam equals that of the incident beam. This requires that after n round-trips, M_T^n be $\pm I$, where I is the unity matrix. Inspection of Equation 3 shows that $M_T^n = (-1)^m I$ whenever

$$n\theta = m\pi . \qquad (5)$$

Here, n and m are any two integers, where n denotes the number of round trips that the beam has undergone and m designates the number of semicircular arcs that the spot pattern produced by the bouncing beam completes on one of the mirrors. As an example, if m=3, then the bouncing beam traverses three semicircular arcs, giving a full angular sweep of 540 degrees before the beam exits the MPC. Equation 5 summarizes the most important design rule for the construction of q-preserving MPCs.

Compact femtosecond MPC Ti:Al_2O_3 laser

We recently developed a compact femtosecond Ti:Al_2O_3 laser based on a novel q-preserving multi-pass cavity design [27]. The laser is all-solid-state, has prismless dispersion compensation with double-chirped mirrors (DCM) [6, 28], a multi-pass cavity (MPC) design to increase the effective cavity length, and tight focusing geometry to enable efficient low-threshold operation.

Figure 16 shows a schematic of the compact MPC Ti:Al_2O_3 laser. A 2-mm-thick Brewster-angled Ti:Al_2O_3 crystal (xtal) was placed in an X cavity between two curved high reflectors (R = 3 cm) and was end-pumped at 532 nm by using a frequency-doubled, diode-pumped Nd:YVO_4 laser. The cavity length was extended by including a MPC that consisted of high-reflectivity curved (M6, R = 2 m) and flat (M7) Bragg reflectors. The beam entered the MPC through a notch on the curved mirror and exited through a second notch on the flat mirror. The MPC was aligned so that the beam bounces formed a circular spot pattern on each mirror. The mirror separation was 23.4 cm, resulting in successive spots separated by 40 degrees along the circular pattern. Starting at the input reference plane indicated as z_{R1} in Figure 16, calculations show that when the bouncing beam makes 9 full round trips during a single transit through the MPC, the q parameter of the Gaussian beam upon exit is preserved and the KLM operating point remains invariant. Because notches were used for coupling the beam into and out of the MPC in our design, only 8 full round trips are completed during a single pass. The remaining round-trip can be completed by retro-reflecting the exiting beam with a curved mirror located at a distance equal to the MPC mirror separation. The radius of curvature of this mirror must be R/2 where R is the radius of curvature of the curved MPC mirror (1-meter curved mirror in Figure 16). This design, scalable to any value of R, always gives a q-preserving MPC, guaranteeing that the parameter of the Gaussian beam returning from the MPC is identical to that at the reference plane z_{R1}. The overall size of the laser was 30

cm x 45 cm. The effective round-trip cavity length was 9.6 m, corresponding to a pulse repetition rate of 31.25 MHz.

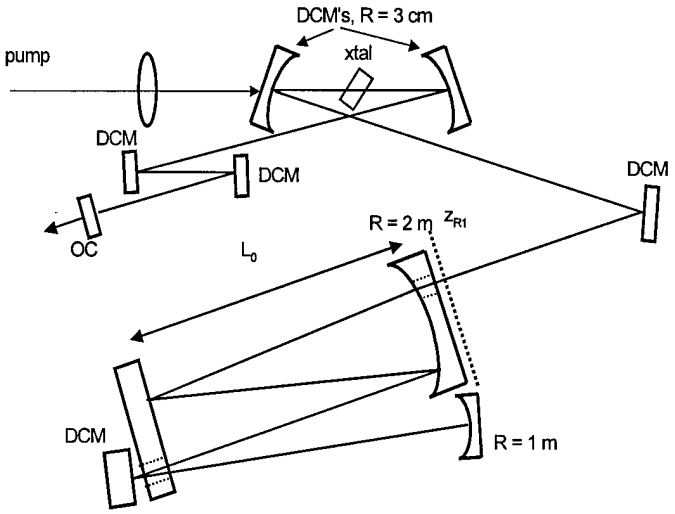

Figure 16. Schematic of the compact prisimless femtosecond Ti:Al_2O_3 laser based on a novel q-preserving multi-pass cavity design.

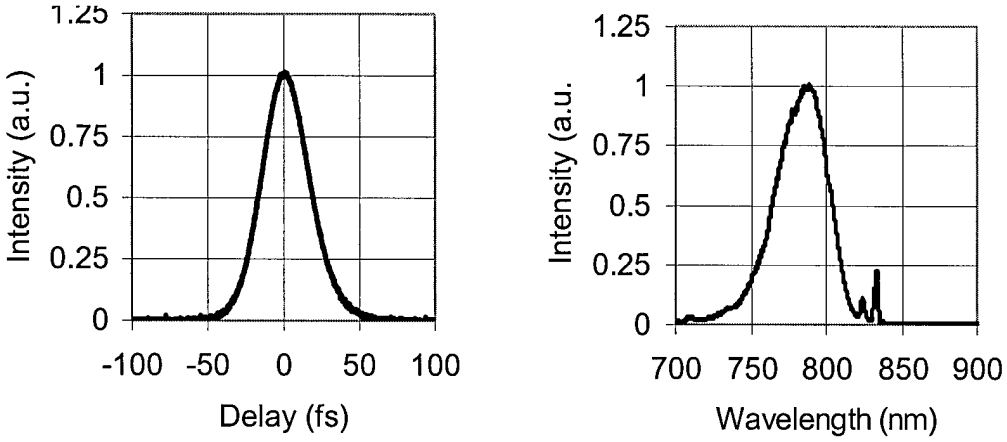

Figure 17. (a) Autocorrelation and (b) spectrum of the femtosecond pulses obtained from the compact prismless MPC Ti:Al_2O_3 laser.

With 1.5 W of pump power, up to 88 mW of mode-locked output power was obtained, corresponding to 2.8 nJ of pulse energy at 31.25 MHz repetition rate. This pump power was chosen because compact, low-cost pump lasers operating with this output power are now available. Figures 17 (a) and (b) show the spectrum and the autocorrelation, respectively, of the pulses obtained with 1.5W of input pump power. The pulse duration (FWHM) was measured to be 23 fs, assuming a $sech^2$ pulse profile. The spectrum is centered around 790 nm with a spectral bandwidth of 40 nm and the time-bandwidth product was 0.45.

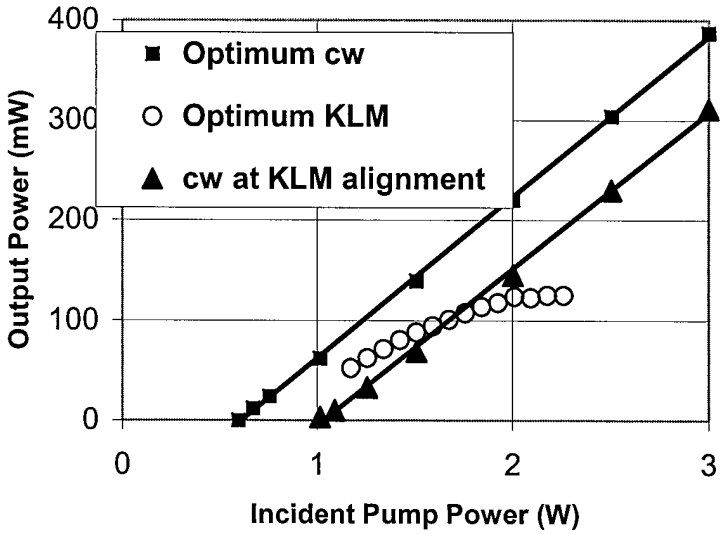

Figure 18. Efficiency data for the MPC Ti:Al_2O_3 laser.

Figure 18 shows the power efficiency curves taken with the MPC Ti:Al_2O_3 laser up to an input pump power of 3 W. Cavity alignment for optimum KLM (shown as open circles) and optimum cw (solid squares) operations are slightly different. As the pump power is increased, the output pulse energy for KLM operation saturates at 4 nJ with 2.3W of input pump power. When the mode-locked operation was stopped, the resulting cw oscillation of the resonator at the KLM operating point is shown as solid triangles in the figure.

Generation of 150 nJ pulses from a multi-pass cavity Ti:sapphire laser

The pulse energies from typical femtosecond Ti:sapphire lasers are limited to a few nanojoules. Higher pulse energies can be obtained by using a cavity dumper within the oscillator, or through external pulse amplification. However, these approaches add complexity and cost to the Ti:sapphire system. A simple and economical approach is to simply scale the laser cavity length and reduce the repetition rate of the laser, resulting in higher pulse energies. For reasons described above, we used a multi-pass cavity laser design to develop a high-energy, extended cavity prismless Ti:sapphire laser [30]. This MPC laser produces pulses at 5.85 MHz repetition rate, with energies as high as 150 nJ and 43 fs pulse duration, which corresponds to 3.5 MW peak power.

Figure 19 shows a schematic of our high-pulse energy laser. The pump is a frequency-doubled Nd:vanadate laser that produces up to 10 W at 532 nm. Unabsorbed pump light is retroreflected back into the crystal to increase the average output power. The laser cavity uses a standard x-folded configuration, with the addition of the MPC within which the beam bounces 48 times.

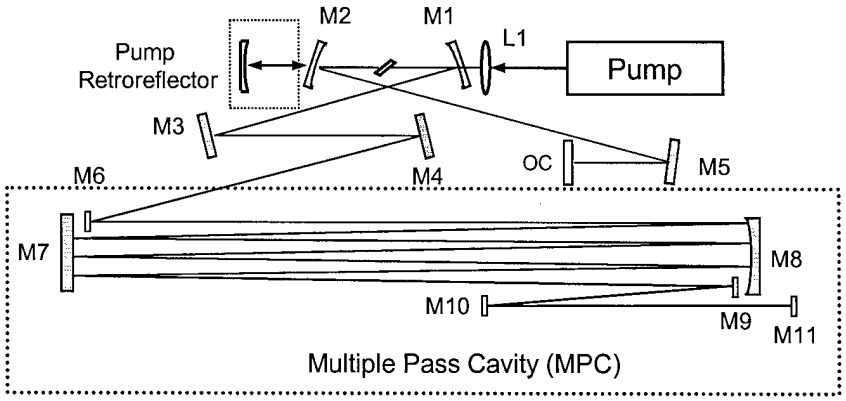

Figure 19. Schematic of the high-pulse energy laser cavity. The shaded mirrors are double-chirped mirrors. Repetition rates of 5 MHz can be achieved using a Multiple Pass Cavity.

The MPC produced a q-preserving transformation to maintain the Kerr-lens modelocking operating point of the unextended laser cavity. The increased pulse energy leads to enhanced self-phase modulation in the crystal, which can lead to instabilities. To balance the self-phase modulation, we increase the negative dispersion by using double-chirped mirrors for the MPC, leading to a net dispersion of -1250 fs^2 after accounting for an additional air path of 48 m.

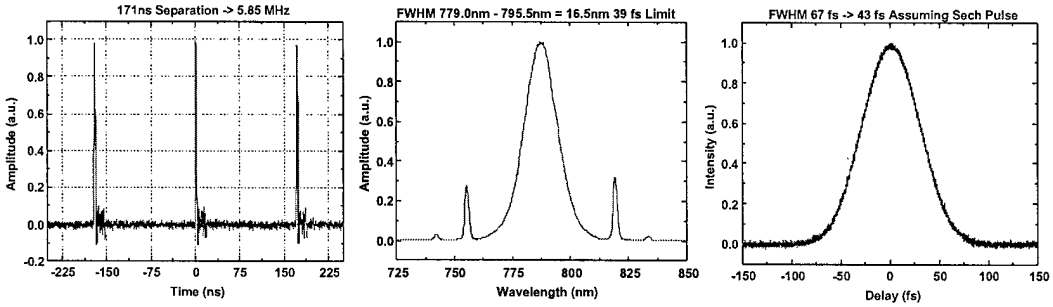

Figure 20. Laser output of the 150 nJ Ti:sapphire MPC laser, measured with a fast photodiode and oscilloscope (a), spectrum (b), and intensity autocorrelation (c).

Figure 20a shows the laser output measured with a fast photodiode and oscilloscope. The oscilloscope trace shows spikes separated by 171 ns, which corresponds to a repetition rate of 5.85 MHz. Figure 20b shows the output spectrum as measured by an optical multichannel analyzer. The spectrum has a bandwidth of 16.5 nm FWHM and is centered at 788 nm. Figure 20c shows the intensity autocorrelation performed with a thin KDP crystal. The autocorrelation shows a FWHM of 67 fs, which corresponds to a 43 fs pulse duration.

This laser could be useful for applications that benefit from high pulse energies, such as harmonic generation, continuum generation, and photonic device fabrication using nonlinear materials processing.

An extended cavity Cr:LiSAF laser pumped by low-cost diodes

In order to make femtosecond solid-state lasers more widely available outside the laboratory, methods of reducing cost while maintaining performance must be developed. A substantial part of the cost of these lasers comes from the solid-state lasers that are used to pumped femtosecond lasers. This problem can be addressed by using materials that are directly diode pumpable. Recent studies have demonstrated Cr:LiSAF as an attractive laser material which can be pumped by very low-cost single-spatial-mode diodes [31,32]. Single-mode laser diodes which emit 50-60 mW at 660-690 nm wavelengths cost only about $20-$50 each. Previous researchers have demonstrated such single-mode diode-pumped Cr:LiSAF lasers; however, the highest pulse energy previously achieved was only 0.14 nJ [31].

We demonstrated a single-spatial-mode diode pumped Cr:LiSAF that uses a multi-pass cavity to obtain higher pulse energies [33]. Two different designs using prisms versus double-chirped mirrors were used for dispersion compensation. This laser achieved pulses of 39 fs duration, 20 nm bandwidth, 8.6 MHz repetition rate, and 0.75 nJ pulse energy using double-chirped mirrors. When prisms were used, the laser produced pulses of 43 fs duration, 18.5 nm bandwidth, and 0.66 nJ pulse energy at 8.6 MHz repetition rate.

Figure 21 shows the schematic of the extended-cavity Cr:LiSAF. Two 50 mW diodes at 663 nm and one 50 mW diode at 685 nm were used to pump the crystal. The diodes were microlensed to produce a circular output beam. The three diodes were collimated and multiplexed by a polarizing beam splitter, yielding a pump beam with a total power of 137 mW incident on the crystal when each diode was driven with only ~120 mA current. The multi-pass cavity consists of one plane double-chirped mirror (DCM) and one 4 m ROC curvature DCM separated by 2 meters, with DCM pickoff mirrors to introduce and extract the beams. The beam made 16 bounces on the MPC mirrors. A saturable Bragg reflector (SBR), similar to that described in [34], was used to start and stabilize modelocking.

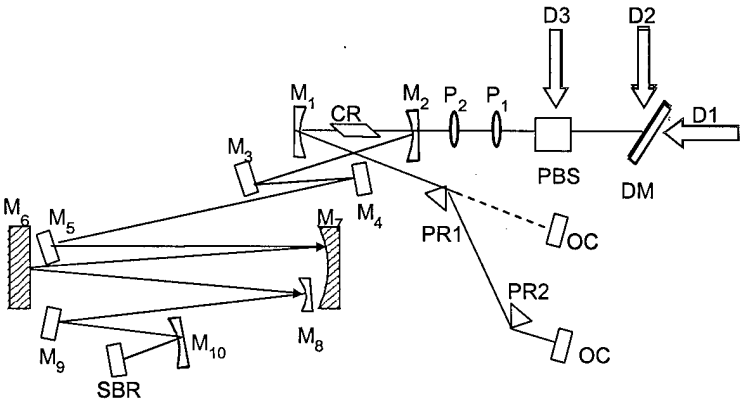

Figure 21. Experimental setup of the extended cavity Cr:LiSAF laser. The components are: pump diodes D1-D3, dichroic mirror DM, wave plate WP, polarizing beam splitter PBS, lenses P1-P2, mirrors M1-M10, output coupler OC.

Figure 22 shows the pulse intensity autocorrelation (a) and spectrum (b) of the extended cavity Cr:LiSAF laser with prisms. The results from the prismless configuration are shown in Figure 23 (a) and (b). This laser could be used for applications requiring moderate pulse energies and short pulses.

Because of the low cost of the diode pump source, the extended cavity Cr:LiSAF laser could potentially be a low-cost alternative to conventional Ti:sapphire lasers. This type of laser technology could also be extremely power efficient.

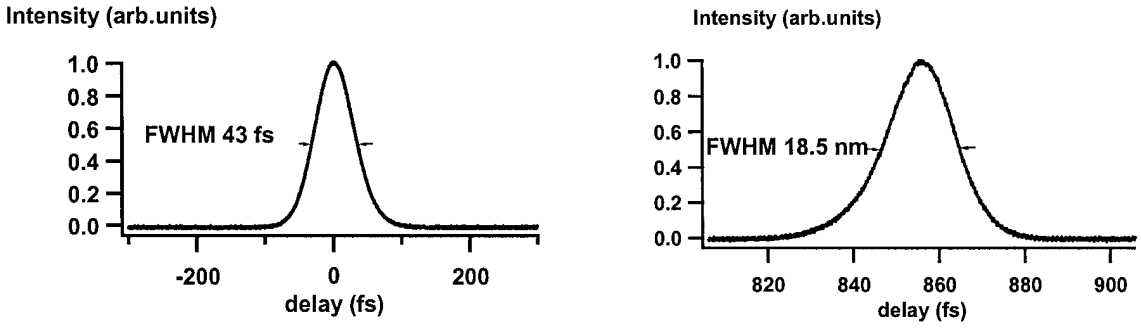

(a) (b)

Figure 22. Intensity autocorrelation (a) and spectrum (b) of pulses from the extended cavity Cr:LiSAF laser with prisms.

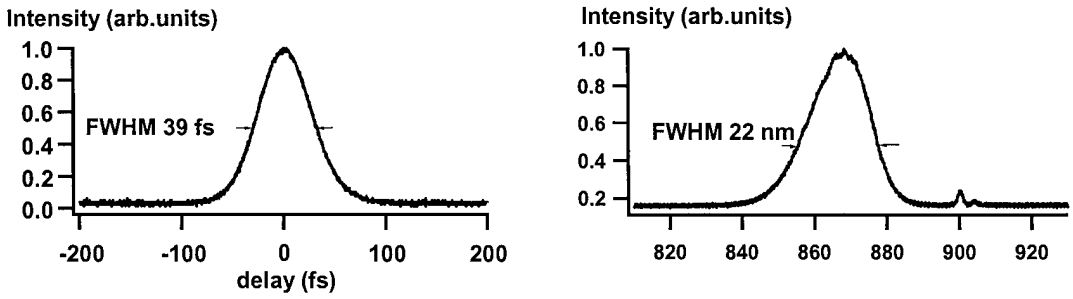

(a) (b)

Figure 23. Intensity autocorrelation (a) and spectrum (b) of pulses from the extended cavity prismless Cr:LiSAF laser.

Continuum generation using multi-pass cavity lasers

High pulse energies enable a wide range of nonlinear processes. A high-intensity pulse focused into a transparent medium will experience spectral broadening due to nonlinear effects such as self-phase modulation and Raman scattering. The resulting white light continuum is a promising broadband light source for applications such as ultrafast spectroscopy [35], optical coherence tomography [36], and optical frequency metrology [1]. The continuum pulses can also be compressed to yield ultrashort high-energy pulses [37].

Recently, there has been considerable interest in using microstructured fibers or tapered fibers for continuum generation. These fibers have small core diameters as well as a shifted zero dispersion wavelength or flattened dispersion that increases the nonlinear conversion efficiencies. The advantage of these fibers is that relatively low pulse peak powers are sufficient to generate ultrabroadband continuum. Continuum can thus be produced directly from the laser oscillator and without the aid of external pulse

amplification. Microstructured fibers typically have an array of air holes that run down the length of the fiber and surround a small silica core. Ranka et al. have used pulses of 100 fs duration and 0.8 nJ pulse energy (8 kW peak power) launched into a microstructured fiber to generate continuum from 390 nm to 1600 nm [38]. A tapered fiber is structurally similar to a microstructured fiber that has large air holes surrounding the core. Tapered fibers are fabricated from standard telecommunications fibers, which are more widely available than microstructured fibers. Using a Ti:sapphire laser, Birks et al. have demonstrated 370-1545 nm continuum generation from tapered fibers [39]. However, tapered fibers are relatively fragile and need to be protected from dust and damage.

If the laser oscillator directly produces high-energy pulses, then there is greater flexibility in the material choice for continuum generation. For example, Baltuska et al. used 40 nJ, 13 fs (3.1 MW peak power) pulses from a cavity-dumped Ti:sapphire laser to generate continuum spanning 500-1000 nm from a single-mode fiber [37. We propose to use the 150 nJ, 43 fs (3.5 MW peak power) MPC laser discussed in the previous section to generate broadband continuum. As in the examples cited above, this approach would not require external pulse amplification to generate continuum. Furthermore, using higher pulse intensities it should be possible to achieve broader bandwidths with lower noise and improved phase coherence.

However, as pointed out in reference [37], pulses of higher energies (on the order of a few tens of nJ for 13 fs pulses) tend to damage standard single-mode fibers. To avoid such damage, we will explore hollow-core fibers to generate continuum. A hollow-core fiber has the advantage of allowing a large diameter mode to propagate, and can therefore withstand higher input intensities. For example, Nisoli et al. have used 4 GW peak power pulses from an amplified Ti:sapphire laser launched into argon-filled hollow fibers to generate a continuum that spans over 300 nm [40]. This result suggests that it may be possible to generate continuum in hollow-core fibers using pulses from our current MPC laser or future MPC designs that generate higher pulse energies.

Increasing pulse energy in MPC lasers: cavity dumping and thermal management

Our current MPC laser can produce record pulse energies of 150 nJ at repetition rates of ~6 MHz. However, for many applications, it is desirable to have even higher pulse energies. We propose to explore methods for increasing pulse energies. We believe that it should be possible achieve pulse energies approach the μJ range.

Cavity dumping is a technique that uses a thin intracavity acoustic-optic element to switch out the laser pulse at regular intervals. The cavity dumper can diffract out a significant fraction of the intracavity pulse energy, greater than possible using standard output coupling, thereby increasing the output pulse energy. Previous work on cavity-dumped, modelocked solid-state lasers has yielded promising results. Our group performed the first demonstration of cavity dumping in a modelocked Ti:sapphire laser several years ago. The cavity dumped laser generated 100 nJ pulses of 50 fs duration [49]. Subsequently, Pshenichnikov et al. demonstrated 60 nJ, 13 fs pulses, also from a modelocked Ti:sapphire laser [50].

The MPC laser has features that overcome many of the limitations which occur with cavity dumping standard lasers. Double-chirped mirrors can be used to compensate for the additional dispersion introduced by the AOM material. Since Bragg diffraction occurs when the optical pulse and the acoustic wave interact, the cavity dumping rise time is governed by the time the acoustic wave takes to traverse the spatial extent of the optical beam. Standard modelocked lasers operate at high repetition rates, so it is necessary to tightly focus the beam onto the AOM in order to reduce the acoustic wave's traversal time through the optical beam. At high energies such tight focusing can damage the AOM material, which limits the achievable pulse energy. The low repetition rate of the MPC laser is especially suitable for

cavity dumping because it relaxes the requirement on the acoustic wave transit time and tight focusing of the beam into the AOM is not necessary.

Pulse energies in our current MPC laser are limited by multiple pulse instabilities that occur at higher intracavity pulse energies [51]. However, this process requires multiple transits of a high-energy pulse in the cavity. With a cavity dumper, the intracavity pulse energy can be allowed to build up to a level that transiently exceeds the stable cw modelocking energy and then switched out before the onset of multiple-pulsing instabilities. Since the MPC laser already has higher intracavity energy than standard lasers, cavity dumping should result in very high-pulse energies generated directly from a laser oscillator. We believe that this strategy could increase the pulse energy achievable from an MPC laser by up to one order of magnitude, approaching the μJ range.

Pulse energy performance might be enhanced by thermal management of the laser crystal. In addition to multiple-pulsing, thermal effects also limit the power that is achievable from solid-state lasers. Since a typical solid-state laser is pumped with a high-intensity beam, there is a significant amount of heat deposited in the laser crystal. The laser mode suffers from thermal lensing, distortions, and stress-optic effects related to thermal expansion. Thermally-induced optical distortions are directly proportional to dn/dT, which is the refractive index variation on temperature, and inversely proportional to the thermal conductivity [52,53]. Thermally-induced stress-optical aberrations are directly proportional to the thermal expansion coefficient and also inversely proportional to the thermal conductivity [52]. Cooling the crystal would reduce these detrimental thermal effects. For example, when sapphire is cooled from 300 K to 77 K, the thermal conductivity increases more than 30 times, dn/dT is reduced by a factor of about 7 and the thermal expansion coefficient decreases by more than an order of magnitude [52].

Experimentally, it was shown by Schulz and Henion that a liquid nitrogen-cooled Ti:sapphire laser's output energy increased from 20 mJ to 80 mJ when the crystal was cooled from 273 K to 93 K [52]. The output power of this laser increased by more than two orders of magnitude when the crystal was cooled from 300 K to 93 K. A study on a cryogenically cooled Ti:sapphire crystal by Zavelani-Rossi et al. experimentally showed that there is a critical temperature, which depends on the pump parameters, below which a probe He-Ne beam's spot size and wave front distortions do not change with temperature [53]. At this critical temperature the probe spot size and distortions converge to the values for which the Ti:sapphire crystal was not pumped. Hence we expect that cooling techniques could substantially increase the output powers and energies produced by MPC lasers.

High-repetition-rate Semiconductor, Microchip and Fiber Lasers

Applications such as high-precision optical sampling systems, microwave signal generation, timing distribution and clocking, and ultrahigh bit-rate optical communication systems require high-repetition-rate sources of transform-limited picosecond and sub-picosecond pulses. Modelocked semiconductor lasers, solid-state microchip lasers and modelocked fiber lasers are all potentially well suited for such applications. They can generate streams of ultrashort pulses at multi-GHz repetition rates with low amplitude and timing jitter.

External-cavity modelocked semiconductor laser

Our modelocked semiconductor laser experiments have utilized diodes fabricated for us by collaborators at NEC. The active chips consist of two sections, a 500-μm gain section and a 50-μm saturable absorber section that is reverse-biased to achieve pulse shortening and that is also modulated electrically to control the pulse timing. In an external cavity approximately 1.5 cm in length this laser produces pulses at a repetition rate of 10 GHz. The configuration is illustrated in Figure 24.

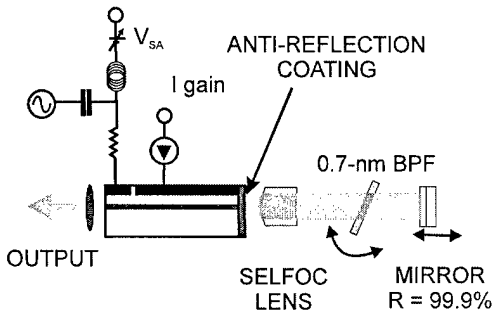

Figure 24: 10 GHz modelocked semiconductor laser

Depending upon the bandwidth of the bandpass filter (BPF), this laser emitted transform-limited pulses with durations in the range 3 - 6 ps at a repetition rate of 10 GHz and an average power of several milliwatts. Following success in obtaining such nice operating characteristics, a principal goal of our experiments has been to reduce the timing jitter in the laser output to the femtosecond level. This required additional cavity stabilization, optimization of the various bias currents and an ultraquiet drive oscillator (Poseiden Shoe Box Oscillator with 5.6 fs jitter). The result has been the achievement of quantum-limited jitter of 86 fs integrated over the full range of 10Hz -5GHz. [54] Recent experiments performed in collaboration with Jun Ye's group at the University of Colorado, in which the cavity was piezo-stabilized to an atomic reference line have further reduced the jitter value to 22fs over the range 1Hz-100MHz. [55]

We have carried out extensive theoretical analyses of how the semiconductor gain and index dynamics influence the noise. [56] It is found that a complicated interplay of dynamics, nonlinearity and dispersion can either increase or decrease jitter by a factor on the order of two. There is also excess quantum noise that results from dynamic non-Hermitian time evolution, similar to that associated with Petermann's K-factor in gain-guided amplifiers. We have also carried out detailed analyses of how perturbations due to spontaneous emission evolve and are controlled by the laser modulation. Lower jitter is achieved with higher cavity Q, higher pulse energy and longer pulses. In general, harmonic modelocking increases supermode noise; but our theory now also predicts that by coherently locking the multiple pulses in such a cavity a higher energy supermode can be created with dramatically reduced jitter. Ultralow jitter would have important implications for rf clocking and the transmission of frequency references over optical fiber communication systems.

Modelocked microchip laser

Solid-state microchip lasers offer perhaps the greatest promise for generating femtosecond pulses at high rep rate. Our approach towards a compact and reliable source of potentially sub-100 fs pulses at greater than 10 GHz repetition rate is a modelocked Cr:YAG microchip laser, as shown in Figure 25. We have already demonstrated continuous wave operation of such a laser, with more than 300 mW of output power from 4W of absorbed pump power and we have shown Q-switched modelocking of this laser using Kerr-Lens or semiconductor saturable absorber modelocking. [57] In this project we propose to develop an optically controlled semiconductor saturable absorber, where in addition to the saturable absorber layer also a modulation layer is integrated, which introduces an externally controllable intracavity loss. We have chosen as a loss modulator free carrier absorption in an InGaAs layer on top of a conventional saturable absorber. The free carrier absorption is broadband and can be controlled by 800 nm light, where Cr:YAG is transparent. Thus the control light can be multiplexed together with the pump light via a dichroic mirror (see Figure 1). Recently, we have demonstrated that the undesired Q-switching can be suppressed by using an active feedback scheme that controls the intracavity loss via the lasers output power [58, 59]. The principle has been demonstrated via feedback to the pump diode current; but it cannot be applied to high-repetition rate lasers. To achieve our goal of a stable, high repetition rate (>10 GHz), cw modelocked microchip laser, we have just begun to use an optically controlled semiconductor element, as indicated in Figure 24, to accomplish both Q-switch suppression and timing control for locking to an rf reference.

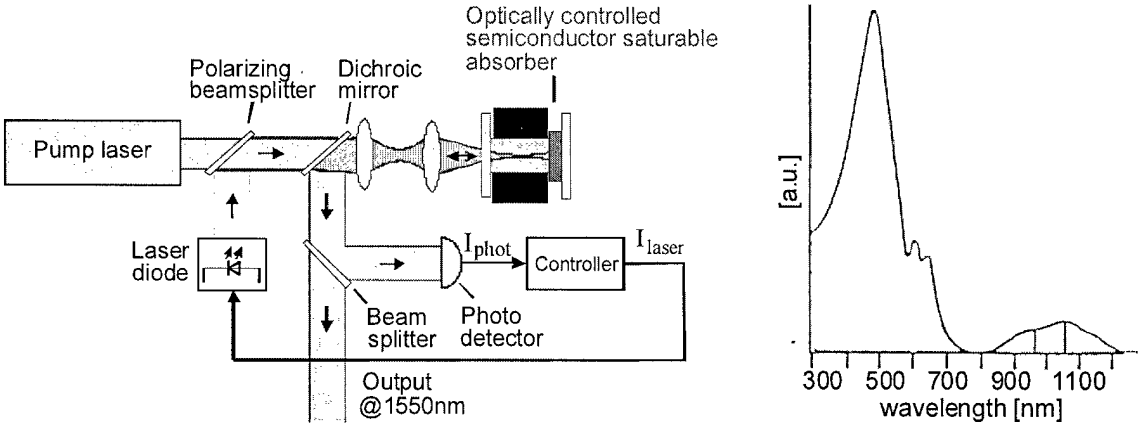

Figure 25: a) Setup of the modelocked femtosecond microchip-laser with feedback loop and optically controlled intracavity loss modulation. b) Absorption spectrum of Cr:YAG.

Harmonically modelocked fiber lasers

Fiber lasers also produce transform-limited picosecond pulses locked to an external frequency reference at GHz repetition rates with low amplitude and timing jitter. They have a potential advantage over semiconductor lasers because of the inherently lower spontaneous emission noise and because of the considerably larger internal pulse energies. To understand and demonstrate this comparison, we have developed a theory for the quantum-limit of timing jitter, identified the characteristic retiming constants that govern the timing jitter for the case of amplitude (AM) and phase (PM) modulation [60], developed a timing-jitter measurement scheme using a balanced microwave homodyne detection scheme with high dynamic range, and built an actively modelocked fiber laser that produces picosecond pulses at 10 GHz whose timing jitter is in fact quantum limited. [61]

The fiber laser setup shown in Figure 26 is arranged in a sigma-type configuration in which only the linear portion is composed of non-polarization-maintaining elements. [62] A faraday rotator at the end of the linear segment ensures that the backward-propagating pulse travels along the orthogonal polarization axis with respect to the forward-traveling pulse. This undoes any polarization rotation and ensures environmental stability.

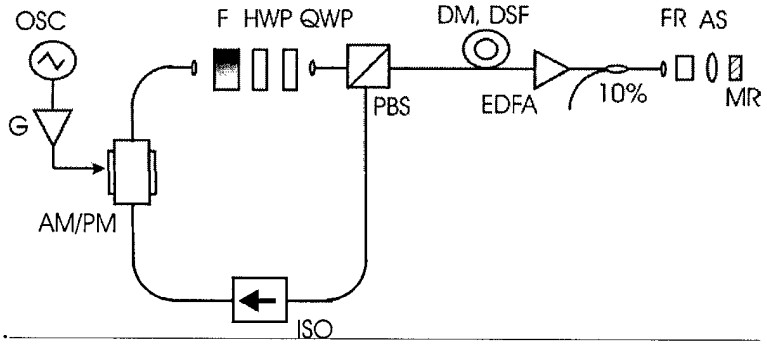

Figure 26. Harmonically modelocked sigma laser with quantum-limited jitter. The OSC is a low noise Poseiden Shoe Box Oscillator

Due to the low gain per unit length of the erbium-doped fiber and the long lengths needed to establish soliton nonlinearities, fiber lasers are generally very long. High repetition rate is achieved by modelocking the cavity at some harmonic, N, of the laser cavity frequency, resulting in N pulses per round trip. This results in a timing jitter spectrum that is more complicated than that for a fundamentally modelocked laser and depends strongly on the pulse-to-pulse correlations. Previous work in the literature on measuring and interpreting the timing jitter has not properly taken these correlations into account. We have shown how the pulse-to-pulse correlations are related to the total timing jitter, developed a theoretical model, and demonstrated experimental confirmation of the model.

The laser produces transform-limited, hyperbolic-secant pulses at 1.5 μm at repetition rate of 10 GHz with pulsewidths from 900 fs to 2 ps, depending on the optical filtering and pump power. The suppression of supermodes in the RF spectrum is typically greater than 70 dB, indicative of excellent laser stability. The laser is locked to the external microwave frequency reference by stabilizing the cavity length using a phase-locked loop (PLL) consisting of a microwave phase detector, control electronics, and a fiber-wound piezoelectric transducer.

The measurement of the laser timing jitter achieved using a residual phase-noise measurement technique is shown in Figure 27.

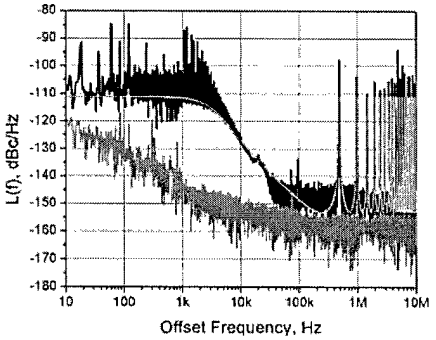

Figure 27: Timing jitter spectrum for the case of amplitude modulation. Upper solid curve, data; lower solid curve, measurement noise floor; dotted curve, theory.

The characteristic spectrum of the jitter at low frequencies (f < 250 kHz) is well understood. However, the significance of, and complete explanation for, the features appearing at harmonics of the fundamental round-trip frequency, referred to as supermodes, had not been previously explained. We have shown that the supermodes are, in fact, aliased versions of the baseband mode and contribute to the overall timing jitter by a factor of $\sqrt{N}$, where N is the harmonic number. This is consistent with the explanation that pulses within the laser cavity are uncorrelated with each other. We confirmed this by measuring the timing jitter by comparing the accumulated timing jitter from one pulse to the next using optical cross-correlation and comparing it with the integrated timing jitter. With this understanding we are now armed to pursue considerable lower jitter. By correlating all of the pulses in the laser cavity by using an etalon or GTI, we should be able to take advantage of the total intracavity energy and reduce the timing jitter reduce by a factor of $\sqrt{N}$.

To further improve our fiber laser pulse source, we are investigating a new higher gain, broader-gain-bandwidth type of fiber amplifier: Bi_2O_3-based erbium-doped glass. With it, we have achieved gain greater than 12 dB over a wavelength range from 1520 to 1600 nm in a fiber only 22.7 cm long. We have also already demonstrated picosecond pulse amplification without pulse broadening, tunable over the full 80 nm range.[63] Sub-picosecond pulses should be more easily achievable with this fiber than with conventional fiber. Shorter overall laser lengths will also make fully coherent, ultralow jitter, harmonic supermodes easier to obtain.

Studies of Ultrafast Phenomena in Materials and Devices

In order to improve designs of devices for applications in lasers, opto-electronics and telecommunications, it is necessary to understand the fundamental properties of materials and device structures. Our focus has been on material and device responses in the wavelength range between 1400 nm and 1600 nm for which we use a tunable, synchronously-pumped, high rep-rate optical parametric oscillator (OPO), producing 150 fs pulses. With the pump-probe technique we obtain information about gain, absorption and index changes, as well as the dynamics of their recovery. Our setup, used with low frequency chopping for heterodyne as well as amplitude modulation, has a measurement sensitivity of ~ 10^{-4} for changes on a femtosecond timescale.

Objects of current studies are: crystalline germanium on undoped silicon, novel quantum well saturable absorbers on semiconductor mirrors (both oxidized and unoxidized) and highly nonlinear calgogenide glass fiber. Pump-probe experiments performed on non-epitaxially grown saturable absorbers are also described in detail in the later section. We propose to continue each of these studies, extend them to integrated structures and to the shorter timescales made possible by our 20 fs Cr:YAG laser or by OPO pulse compression in fiber. We also propose to revisit active waveguides and to study dynamics in novel integrated semiconductor optical amplifier (SOA) circuits.

Germanium saturable absorbers on silicon mirrors

A 543-nm-thick film of crystalline germanium on an undoped silicon wafer was characterized to determine its suitability for use as a broadband ultrafast saturable absorber. The maximum absorption of the film at 1540 nm is ~ 8.5%. Pump-probe traces as a function of incident fluence are shown in Figure 28. The fast component, due to spectral hole burning and thermalization of carriers, recovers quickly and is a large percentage of the overall signal. However, there is still a long-lived component of the signal, due to recombination and thermal effects. Future studies of these effects as a function of growth and fabrication conditions will help determine the optimum design for a broadband saturable absorber. These novel materials are fabricated for us by Prof. Fitzgerald's group at MIT. The development of a such a

saturable absorber material, compatible with silicon technology, would be particularly valuable because the combination of silicon and SiO_2 also provides the basis for a variety of high index contrast devices.

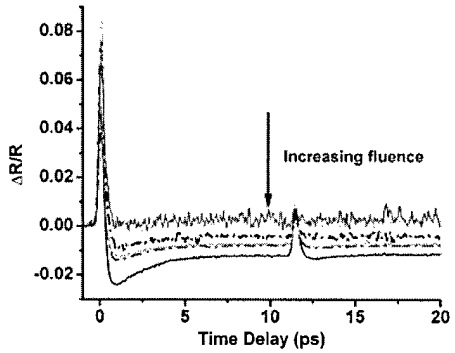

Figure 28: Pump-probe trace of 543 nm Germanium film at 1540 nm and as a function of fluence.

InP-based SBRs

High-modulation-depth InP-based saturable Bragg reflectors (SBRs), designed for use in a high repetition rate laser systems, were fabricated by Professor Kolodziejski's group. They consist of 12 InGaAs quantum wells in a λ–thick layer of InP. This is grown on top of an MOCVD-grown mirror consisting of a 22-pair GaAs/AlAs Bragg stack, centered at 1550 nm with a 100 nm bandwidth. Additional InP was overgrown on the structure to enhance two-photon absorption, which we have found can help stabilize lasers against Q-switching instabilities [64]. Structures with either antireflection or resonant coatings to enhance the modulation depth have been investigated. Figure 29 shows a pump-probe trace of the resonantly coated structure, in which a maximum modulation depth of 20% has been achieved.

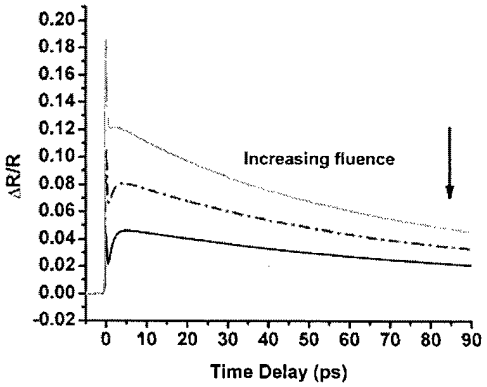

Figure 29: Pump-probe trace of a high-modulation-depth SBR at 1575 nm.

The recovery time of this device is ~ 43 ps, due to the high lattice mismatch between the InP and the GaAs. New structures are now being grown for the purpose of achieving an enhanced ultrafast component and faster overall recovery.

Two-color pump-probe

We have also performed a variety of two-color pump-probe studies, using the 800 nm pump pulses as well as the OPO output. Because the OPO is synchronously pumped, these two colors have less than 20 fs of timing jitter [65] between them. In addition, it is possible to perform two-color pump probe with

the OPO signal and idler. Microstructured fiber [66] and a Fabry-Perot device have been studied using this technique. The Fabry Perot device consisted of 1 μm of polysilicon on a 1 mm quartz substrate, forming a Fabry Perot. The Ti:sapphire laser was used as the pump and the OPO as the probe. The Ti:sapphire generated free carriers in the sample, causing the index to change slightly. This in turn, leads to a shift of the resonances of the Fabry-Perot, causing a change in transmission as a function of wavelength. From this pump-probe experiment, a carrier density of 3 x 10^{18} /cm^3 produced an index change of ~0.15%, a number that agrees well with values in the literature. Further experiments will be directed toward demonstrating the utility of such structures as rapidly, all-optically switchable filters.

Semiconductor optical amplifiers are also being revisited for all-optical switching applications. They known to have large optical nonlinearities and rapid response times that make them attractive for a variety of wavelength shifting and optical logic gate applications. We have previously performed extensive studies of both index of refraction dynamics and gain dynamics in standard cleaved facet device.[67] Typical results are shown below. They show promising ultrafast components as well as not so rapid components related to carrier population dynamics.

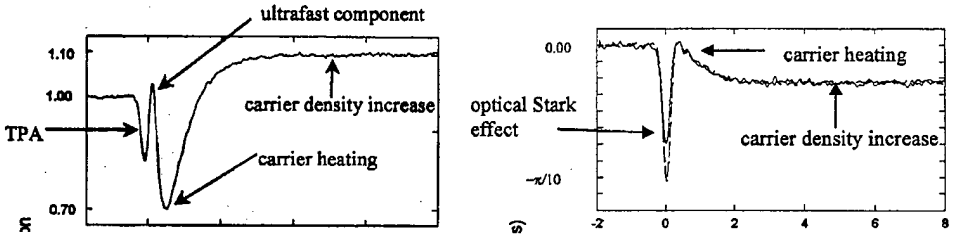

(a) (b)

Figure 30: Pump-probe traces of (a) gain and (b) index dynamics in an InGaAsP quantum well SOA

New integrated devices are being designed and fabricated by collaborators Rajeev Ram and Leslie Kolodzjieski at MIT. Both Mach-Zehnder and Ultrafast Nonlinear Interferometer (UNI) [68] geometries will be fabricated and tested in multi-gate configurations.

Calcogenide glasses and Omniguide fiber

The incorporation of highly nonlinear calcogenide materials into Omniguide fiber [69] promises to greatly reduce the powers and fiber lengths needed for nonlinear switching. We have begun a collaboration with colleagues at Omniguide Communications, who are developing this novel fiber technology, to study the ultrafast nonlinear characteristics of the key materials. Onmiguide fiber consists of concentric cladding layers that act as perfect mirrors for light of all wavelengths in the core. The design of the particular layer dimensions can also be used to tailor the dispersion characteristics of the fiber guide. We have begun initial experiments on $Ge_{33}As_{12}Se_{55}$ whose constituent ratios have been chosen to set the bandgap of the material close to, but far enough above to avoid losses from, the two-photon energy of pulses at 1.5μm. We will study the nonlinear index n_2 and the two-photon absorption coefficient β as a function of wavelength. Experiments re being carried out using spectral interference pump-probe as well as the Z-scan method. As Omniguide fibers with GeAsSe cores are fabricated we will evaluate their performance in all-optical switch configurations.

Phase sensitive nonlinear optics

With the arrival of laser pulses consisting of only a few optical cycles, attention has been drawn to effects that not only depend on the electric field envelope, but also on the phase between the rapidly oscillating carrier wave and the envelope. Different approaches have been used for detecting this carrier-envelope (CE-) phase φ_{CE}. Recently, it has been shown that a promising candidate is carrier-wave Rabi flopping [70]. Carrier-wave Rabi flopping is defined as the regime in which a resonant excitation of a two-level system is so strong, that significant inversion is generated during one optical cycle [71]. This regime occurs when the Rabi frequency approaches the carrier frequency. It has been demonstrated that the corresponding Mollow sideband radiation emitted from the two-level system at different harmonics can interfere with each other or with the bulk or surface generated second harmonic radiation, producing a CE-phase sensitive photocurrent in a detector [72]. Here, we want to investigate the off-resonant excitation of a two-level system, i.e., in the weak-field limit there is no excitation of the system at all, which may lead to a phase sensitive inversion after passage of the pulse in the strong field limit. The phase sensitive inversion can be directly probed optically or it can be read out electronically by an applied field, resulting in a compact electronic phase detector. A portion of the detector current is directly proportional to the carrier-envelope phase.

Figure 31 shows the inversion left in a two-level atom after irradiation with a T_{FWHM} =5fs long, sinc-shaped pulse, which is a fairly good description of recently generated few-cycle laser pulses [4]. The result is shown for two values of the carrier-envelope phase $\varphi_{CE}=0$ in (a) and $\varphi_{CE}=-\pi/2$ in (b) for a detuning of the laser pulse from the resonance of $\Delta=0.886/T_{FWHM}$ and a maximum field strength of $E_{max}=6$ V/nm. The dynamics of the two-level system is found by numerically solving the Bloch equations.

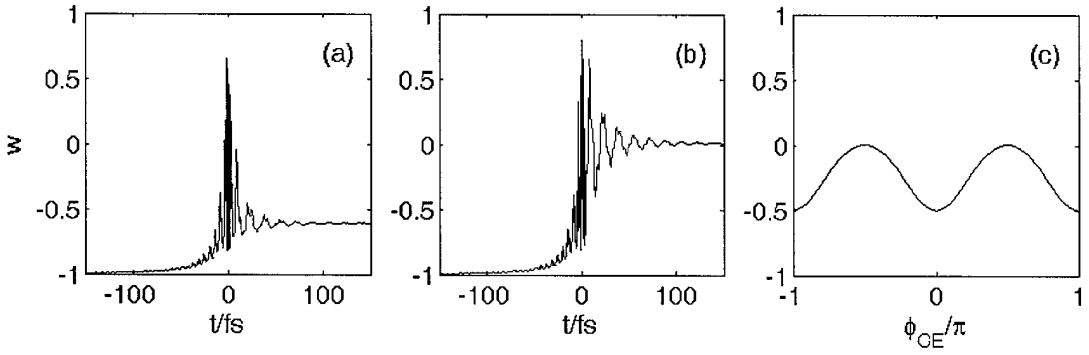

Figure 31: Inversion w for a two-level atom interacting with a 5 fs optical pulse: (a) time evolution for $\varphi_{CE}=0$, (b) time evolution for $\varphi_{CE}=-\pi/2$, (c) phase dependence of the remaining

Figure 31(c) shows the phase dependent population after passage of the pulse, and it shows that the inversion remaining in the system is modulated with twice the CE-frequency. This occurs because the Bloch equations are invariant with respect to simultaneous inversion of the electric field and the dipole moment. Thus, the inversion is invariant.

The inversion can be detected optically, either by an additional probe beam or by the short wavelength spectral components of the pulse itself that are resonant with the two-level system and delayed from the excitation part of the pulse. It is even more appealing to extract the modulated inversion from a diode-like structure in form of an external current. Experimental investigations of these possible novel electronic phase detection schemes are in progress.

Nanoscale scanning probe spectroscopy

We have recently been developing a scanning probe microscope apparatus with capability for apertured-tip near-field microscopy, apertureless probe scanning for photon-tunneling microscopy and topographical surface force microscopy. The ultimate goal is to use these techniques to study ultrafast effects with nanoscale spatial precision. Initial projects have focused on developing and calibrating the methods. A recent objective was to study perturbations of microphotonic circuits by scanning tips. In particular, we studied perturbations on the guided mode of a microphotonic ring resonator. A near field microscope was used to control the distance between a flat-tipped micro-fiber and an unclad ring resonator (see Figure 32a). As the microtip fiber optic approaches the ring resonator, it produces a shift of the center frequency of the ring (see Figure 32b). This tuning mechanism provides a calibration of the effects of a tip on guided and/or resonant modes. It is already proving useful for characterizing microphotonic chips being fabricated by other groups at MIT and for testing novel micro-mechanical electro-optic device designs.

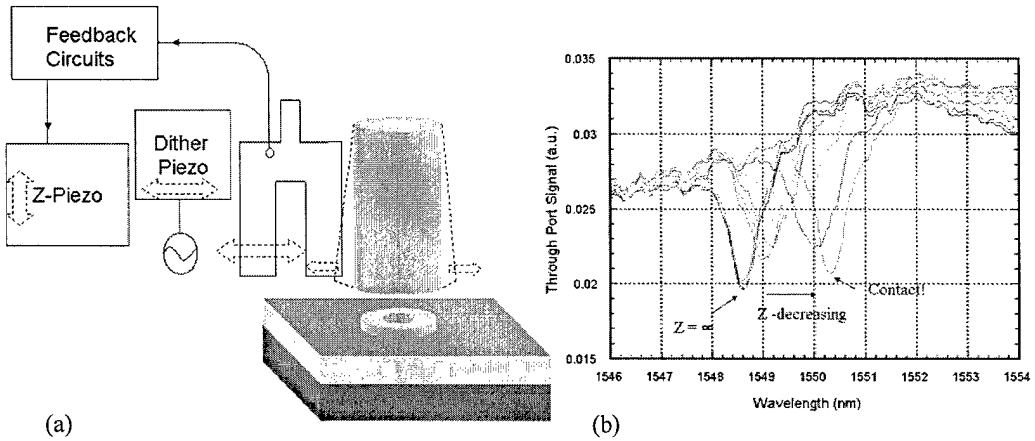

Figure 32. (a) Simple schematic of tuning apparatus. Tuning fork signal is monitored to maintain the distance of probe from surface of ring. (b) Transmission data from the through port of ring resonator for various positions of the probe. The left-most resonances are those with no perturbation, while the progression of red-shifted resonances demonstrate increasing perturbation of the ring resonator.

For the purpose of studying micro-photonic circuits the near-field microscope can also be used in photon scanning tunneling microscopy mode (PSTM). Since the light in a waveguide is generally totally internally reflected, it cannot be directly observed in the far field. However, if a probe is brought in the near field of the waveguide, its evanescent field can be detected since a small amount of the guided light will "tunnel" into the probe. Combined with interferometric techniques, this allows us to detect the phase and amplitude of the guided mode inside of the waveguide. Such newly accessible information about the modes inside of the waveguide may help to resolve questions of coupling and loss in complex devices such as multi-stage ring resonator filters. The transmission third-order ring resonator filter can be seen in Figure 2.

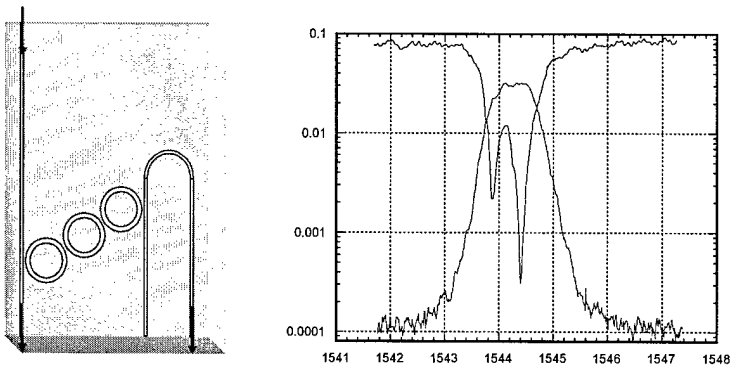

(a) (b)

Figure 33. Schematic and transmission spectrum of third order ring resonator. The through-port and drop-port signals are displayed in red and blue respectively.

The double-peaked characteristic of the through port was unexpected and has led to new understanding and a reevaluation of multi-ring filter design. Additionally, correlation of the topography of the waveguide with the mode amplitude of a waveguide can help to pinpoint problematic artifacts in such devices.

Photonic crystal devices can also benefit from such studies. PSTM can help to reveal the physics behind complex defect states and the Bloch waves excited in photonic crystals. Figure 34 shows a collection mode image of a two-dimensional photonic crystal light emitting diode consisting of a hexagonal lattice of 100nm diameter holes. These holes are clearly resolved with the near field microscope demonstrating the high spatial resolution achievable. Propagation in such structures is characterized by complicated "photonic crystal bands." PSTM will make it possible to map the photonic bandstructure directly and to study the resonance and propagation of light, especially short pulses in a variety of interesting photonic devices. Preliminary 2-D resonators, slow wave structures and superprisms are currently being fabricated by the Kolodziejski group for future studies. We will use our scanning probe, and once we have successfully fabricated and tested photonic crystal waveguides PSTM studies will be a possibility.

(a) (b)

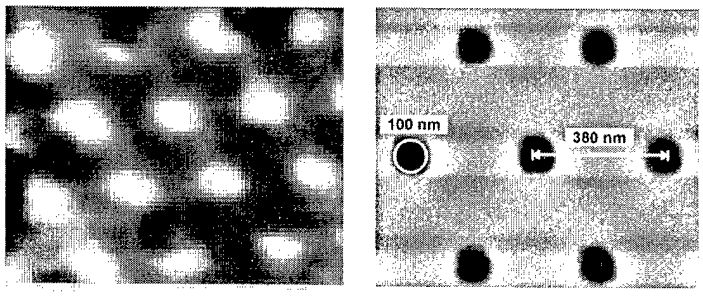

Figure 34: a) Sub-wavelength near-field image of PBG LED taken in oblique reflection/collection geometry. b) The corresponding SEM image of the same sample. The hexagonal lattice formed by the holes can be clearly seen.

On a molecular scale we are also using the different near-field modalities of our instrument to study the properties of nanotubes and nanotube devices. An important feature of the near-field microscope in this case is its ability to correlate topographical information with optical signals. This is helpful in order to resolve a change in physical properties along the nanotube. In Figure 35 the topography of a 3-nm-diameter single wall carbon nanotube, acquired using the near-field probe. The lateral resolution of the nanotube is consistent with approximately 50nm spatial resolution. Next we perform photocurrent and Raman studies of such nanotubes.

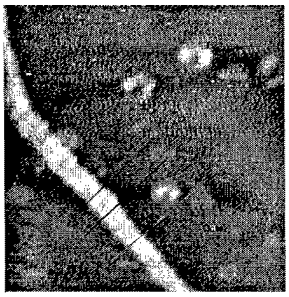

Figure 35: Topography image of a 3nm diameter single wall carbon nanotube. NSOM topography measurement of 2.8 +/- 0.5nm is consistent with AFM measurements of diameter.

Non-epitaxially grown saturable absorber devices for laser mode locking

Epitaxially grown semiconductor saturable absorbers are part of a well-established technology for generating stable, self-starting pulses in solid-state lasers. These devices, known as semiconductor saturable absorber mirrors (SESAM) or saturable Bragg reflectors (SBR), typically consist of semiconductor quantum wells grown in a semiconductor mirror structure by molecular beam epitaxy (MBE) [34,73,74]. SESAMs and SBRs have been very successful in mode-locking solid-state lasers, helping to start and support few cycle pulses in a Ti:sapphire laser[75]. However, they suffer from some disadvantages, such as lattice matching constraints that limit the choice of semiconductor materials as well as the need for a complicated, expensive fabrication system. In addition, the bandwidth of these devices is typically limited and extensive post-processing is required to fabricate broadband devices.

Non-epitaxially grown saturable absorbers based on semiconductor nanocrystallites doped into silica films are a low-cost, simple, and versatile technology for mode-locking applications. In our initial experiments, we developed non-epitaxially grown, RF sputtered saturable absorber devices and applied them to self-starting Kerr lens mode-locking (KLM) in a Ti:sapphire laser[76]. The saturable absorber devices consist of InAs nanocrystallites doped into SiO_2 films and deposited on sapphire substrates using magnetron and non-magnetron radio frequency (RF) sputtering systems.

RF sputtering is an inexpensive, simple device fabrication technique that offers flexibility in the choice of semiconductor dopant and substrate materials. [77-79] This technique allows the deposition of semiconductor-doped silica films onto almost any substrate with no lattice matching constraints. A variety of semiconductors can be chosen as the dopant. Changing the semiconductor dopant and nanocrystallite size enables control of the optical absorption edge. The linear absorption coefficient is directly proportional to the doping density, and the total absorption can easily be scaled by changing the film thickness. The broad nanocrystallite size distribution leads to a broad bandwidth of operation. Finally, these semiconductor-doped silica films can be deposited with much higher doping densities than bulk semiconductor-doped glasses, enabling simple deposition in a thin layer on a variety of substrates

including mirror structures. It was found that rapid thermal annealing (RTA) in nitrogen from 500-750°C was an effective method of controlling the absorption saturation dynamics of the saturable absorbers [80]. In Ti:sapphire, self-starting 25 fs pulses were obtained with a bandwidth of 53 nm and tuning range of 80 nm. The saturation fluence of these devices was measured to be 25 mJ/cm^2, which is too high to enable saturable absorber mode-locking without KLM and also limits the minimum achievable pulsewidth.

More recently, the focus of our investigations was to comprehensively characterize the linear and nonlinear optical properties of these devices in order to develop guidelines for designing semiconductor-doped silica film saturable absorbers with optimized saturation fluence for a given solid state laser system. The influence of fabrication parameters on the optical properties of the saturable absorber devices was measured using linear transmission and pump probe experiments to determine the most important factors impacting device performance.

Measurement of nonlinear absorption cross-section and dynamics

Preliminary investigations examined the influence of nanocrystallite size on the absorption saturation dynamics in InAs-doped silica films. It has been shown [71,81,82] that varying the ratio of semiconductor to glass on the target can be used to control the nanocrystallite size in the sputtered film. Larger semiconductor to glass ratios result in larger nanocrystallite sizes in the deposited film, shifting the optical absorption edge to longer wavelengths. The effect of varying the ratio of InAs to SiO_2 on the size of the InAs nanocrystallites in the silica films was tested. We collaborated with Paul Mak and Professor Michael Ruane at Boston University to deposited films with ratios of 3% InAs/97% SiO_2, 10% InAs/90% SiO_2, and 40% InAs/60% SiO_2 on sapphire substrates using a magnetron RF sputtering system. The films were subsequently annealed in nitrogen at 600°C. Linear transmission measurements (Figure 36) revealed a shift of the absorption edge to longer wavelengths for higher InAs/SiO_2 ratios, as expected. The absorption edge is ~950 nm for the 3% InAs/97% SiO_2 film, ~1200 nm for the 10% InAs/90% SiO_2 film, and ~1700 nm for the 40% InAs/60% SiO_2 film. Varying the semiconductor to glass ratio is a simple and effective way of controlling the nanocrystallite size in the sputtered films, enabling fabrication of films for operation at different laser wavelengths over a broad range with only a single semiconductor material.

Pump-probe experiments were performed on these films to examine the dependence of the saturation fluence on nanocrystallite size. A novel pump-probe system with independently tunable pump and probe wavelengths from 700 to 1000 nm was developed, based on our 5.5 fs Ti:sapphire laser. The time resolution of this system was 17 fs. The magnitude of the measured pump-probe signals can be shown to be inversely proportional to the saturation fluence. The results of pump-probe measurements at 800 nm are shown in Figure 37.

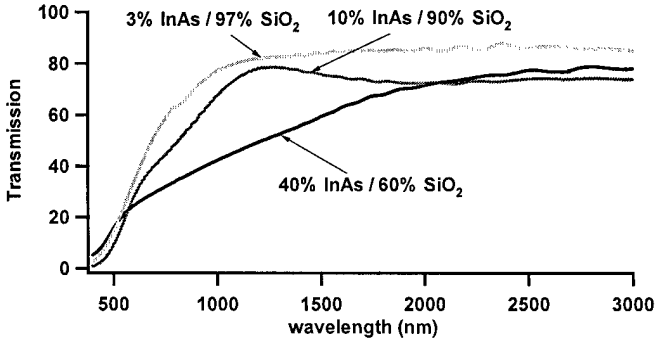

Figure 36. Linear transmission measurements for films with different InAs/SiO_2 ratios, revealing a shift of the absorption edge towards longer wavelengths with higher ratios of semiconductor to glass.

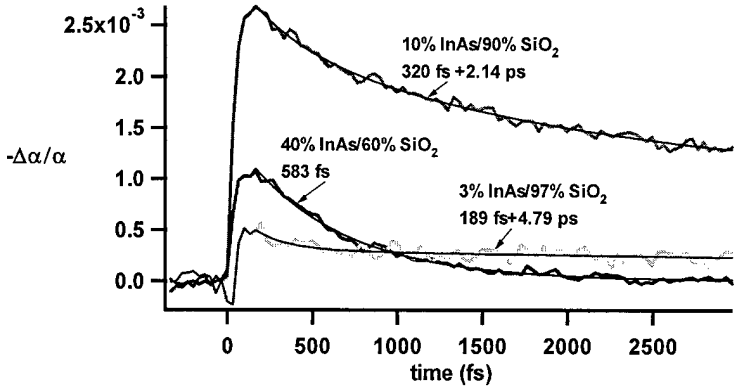

Figure 37. Degenerate pump-probe measurements at 800 nm on InAs-doped silica films with different InAs/SiO_2 ratios. The black lines show the results of fitting the data with exponential or double exponential functions, and the relaxation time constants are labeled for each curve.

From this figure, it can be seen that the 10% InAs/90% SiO_2 film has the lowest saturation fluence at 800 nm (29.5 mJ/cm^2). This motivated experiments to explore the wavelength dependence of the saturation fluence in these films with the tunable Ti:sapphire-based pump-probe system. We examined the saturation fluence near the absorption edge of a 10%InAs/90% SiO_2 film in a degenerate pump probe measurement at wavelengths of 750, 800, and 925 nm (Figure 38). The saturation fluence of this film decreased with increasing wavelength (decreasing to 9.3 mJ/cm^2 at 925 nm), demonstrating that operation close to the absorption edge is desirable to minimize the saturation fluence.

A pump-probe system operating at 1.5 μm was subsequently used to measure the dynamics of the 40% InAs/60% SiO_2 films near their absorption edge of ~1.7 μm. The pump-probe system was based on a Ti:sapphire-pumped OPO generating 150 fs transform limited pulses at an 82 MHz repetition rate, with wavelengths tunable between 1.4 and 1.6 μm. The results of these measurements are depicted in Figure 39.

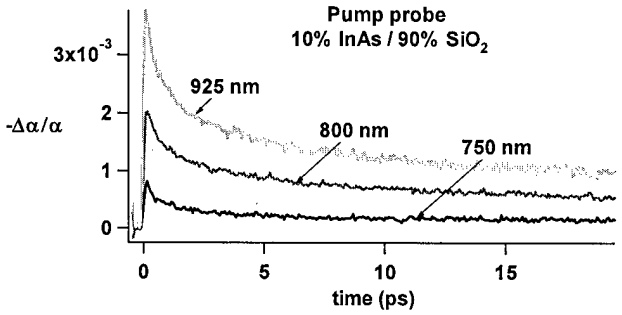

Figure 38. Degenerate pump probe measurement of a 10% InAs/90% SiO_2 film as a function of wavelength, showing a decrease in saturation fluence with excitation closer to the absorption edge.

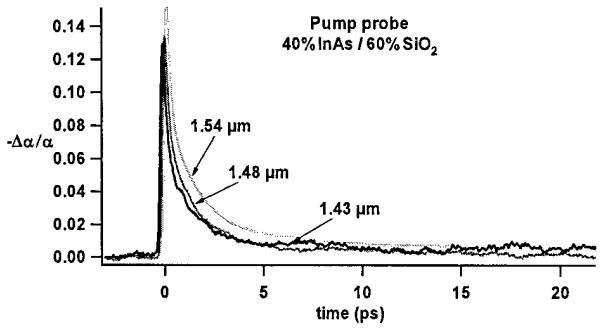

Figure 39. Tunable degenerate pump-probe measurements at wavelengths of 1.54 μm, 1.48 μm, and 1.43 μm on a 40% InAs/60% SiO2 film. A saturation fluence of 640 μJ/cm2 at 1.54 μm was measured.

These measurements show that the saturation fluence decreases with wavelength in this longer wavelength range as well. A saturation fluence of 640 $\mu J/cm^2$ at 1.54 μm was measured in these experiments, significantly lower than the 72 mJ/cm^2 saturation fluence measured on the same film at 800 nm. This is expected since the 1.54 μm wavelength is much closer to the absorption edge. However, this saturation fluence is also significantly lower than the 9.3 mJ/cm^2 saturation fluence measured at 925 nm on the 10% InAs/90% SiO_2 films, even though the wavelengths are at similar distances from the absorption edge. The increase in nanocrystallite size between the 40% InAs/60% SiO_2 films and the 10% InAs/90% SiO_2 films is responsible for the decrease in saturation fluence; the mechanism by which this occurs will be discussed further below.

Influence of Materials Fabrication Parameters on Absorber Performance

The annealing temperature of 10%InAs/90% SiO_2 films was varied to determine the effect of RTA on the nonlinear absorption saturation dynamics. Annealing is expected to modify the surface properties of the nanocrystallites; nanocrystallites with better surface properties are anticipated to have lower saturation fluence. Figure 40 depicts the changes in the measured pump-probe signal at 800 nm as a function of annealing temperature for 10% InAs/90% SiO_2 films annealed for 60 seconds in nitrogen.

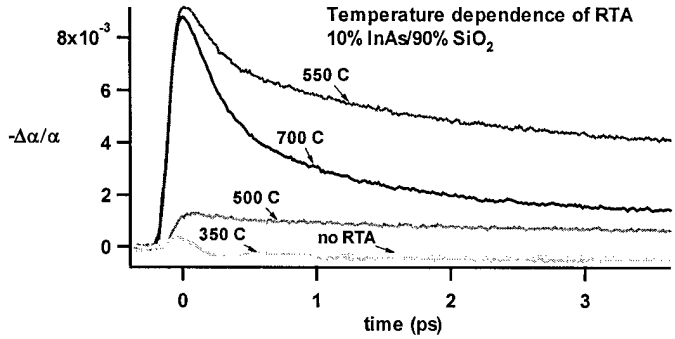

Figure 40. Degenerate pump probe measurement of a 10% InAs/90% SiO2 film at 800 nm as a function of rapid thermal anneal temperature. Discrete changes in the dynamics as a function of annealing temperature are observed.

Distinctive changes in the absorption saturation dynamics were observed as the annealing temperature was varied from 350-700°C, including a large decrease in the saturation fluence between 500 and 550°C. Overall, higher annealing temperatures seem to be effective in improving the surface quality of the nanocrystallites and thereby reducing the saturation fluence, as previously demonstrated [80].

The glass matrix surrounding the nanocrystallites is expected to strongly affect their surface properties and ultrafast dynamics, and therefore experiments to investigate the dependence of the saturation fluence on the glass matrix composition were performed. Films with InAs nanocrystallites doped into a borosilicate glass matrix in a 10% InAs/90% borosilicate glass ratio and deposited on sapphire substrates were fabricated to test the dependence of the absorption saturation dynamics on the glass matrix composition. Pump-probe measurements on these films demonstrated that unlike the SiO_2-based films, the pump probe signal did not change discretely with annealing temperature, instead increasing continuously as the RTA temperature increased (Figure 41). However, at high annealing temperatures the dynamics were very similar to those measured with a SiO_2 matrix, and there was no significant improvement in the saturation fluence.

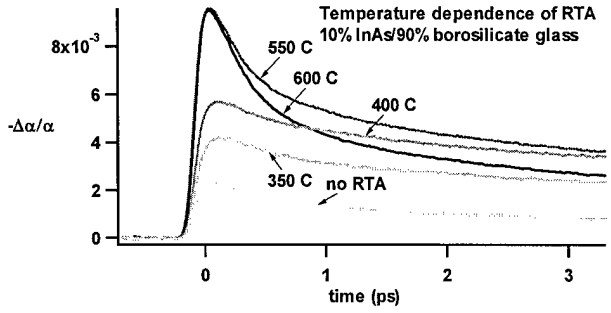

Figure 41. Degenerate pump probe measurement of a 10% InAs/90% borosilicate glass film at 800 nm as a function of rapid thermal anneal temperature

We believe that the difference in annealing temperature dependence between films fabricated with InAs doped into a SiO_2 matrix and films fabricated with InAs doped into a borosilicate glass matrix can be explained by examining the different melting points of the composite films and their relation to the annealing temperature. The surface properties of the nanocrystallites are expected to vary differently with RTA temperature for the two film compositions, influencing the ultrafast dynamics. This demonstrates that the choice of glass and annealing temperature has an effect on the absorption saturation dynamics that must be considered when designing non-epitaxially grown semiconductor-doped silica films.

Guidelines were formulated from the above experimental results to optimize the saturation fluence of semiconductor-doped silica film saturable absorbers for a given laser system. By comparing the minimum saturation fluence of 10% InAs/90% SiO_2 films with 40% InAs/60% SiO_2 films, it can be seen that films with larger nanocrystallites have significantly lower saturation fluence than those with smaller nanocrystallites. It is also clear that the films should have an absorption edge close to the laser wavelength, since this also lowers the saturation fluence (Figure 38). Therefore, the semiconductor material and semiconductor/glass ratio should be chosen to satisfy these two criteria for a certain operating wavelength. Finally, the annealing temperature should be above 550°C for strong absorption saturation based on the results displayed in Figures 40 and 41; however, the optimum temperature may vary for different semiconductor and glass materials. The carrier relaxation time can also be tailored for a particular application by varying the annealing temperature.

These guidelines were applied to design semiconductor-doped silica film saturable absorbers for self-starting mode-locking in a Cr:forsterite laser operating at 1.26 μm [76,83]. The linear and nonlinear optical properties of the 40%InAs/60% SiO_2 films described above were suitable for this application. Films with a saturation fluence of 1.07 mJ/cm^2 at 1.26 μm were fabricated, enabling self-starting KLM with 91 nm bandwidth and pulse durations of 25 fs measured by interferometric autocorrelation (Figure 42).

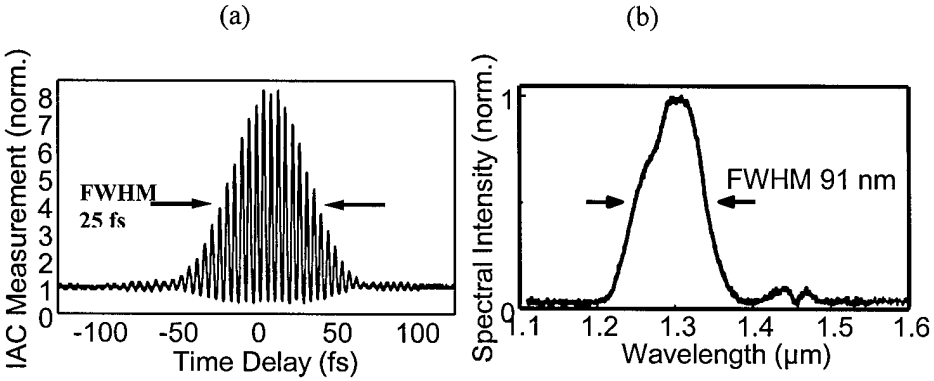

Figure 42. Interferometric autocorrelation (a) and spectrum (b) of self-starting KLM in Cr:forsterite using non-epitaxially grown InAs-doped silica films. Self-starting 25 fs pulses with a bandwidth of 91 nm were generated.

We believe the relatively high saturation fluence in semiconductor-doped silica films can be explained by their fast polarization dephasing times. It has been shown that the dephasing time in quantum dots increases with the nanocrystallite size and surface quality, excitation wavelength relative to the band edge and temperature.[84] From our experimental results, a dependence of the saturation fluence on the nanocrystallite size, annealing temperature (which should influence surface quality) and the excitation wavelength relative to the absorption edge was observed. This indicates that the fast polarization dephasing time in RF sputtered semiconductor-doped silica film saturable absorbers may be the primary limitation in achieving lower saturation fluences and better self-starting performance.

Saturable Absorber Device Design

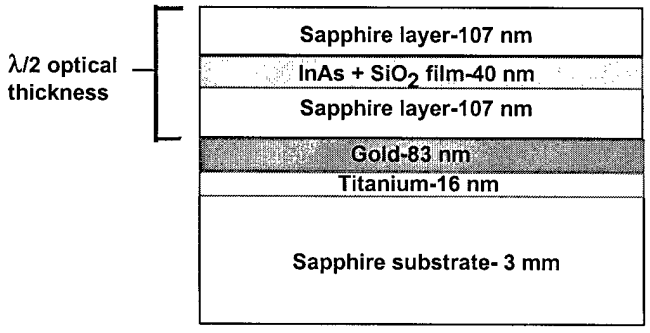

Figure 43. Schematic of the reflective saturable absorber device.

Limitations in saturation cross section can be overcome by implementing novel device designs to reduce the saturation fluence. One method is to design a reflective saturable absorber device incorporating

semiconductor-doped silica films. A standing wave is formed in a laser cavity when an electromagnetic wave is reflected from a mirror; by placing the semiconductor-doped film at the peak of the standing wave, the effective saturation fluence can be reduced by a factor of four.

A promising design is based on sandwiching an InAs-doped film between sapphire spacer layers on top of a gold mirror, all deposited by rf sputtering. Devices based on this design (Figure 43) were previously fabricated in the non-magnetron sputtering system at Lincoln Laboratories, but were not successful in self-starting mode-locking in a Ti:sapphire laser, most likely due to lack of precision in the thickness of the deposited layers as well as possible problems with the morphology of the sapphire-gold interface that reduced the reflectivity of the devices. We expect that we can control the layer thickness much more precisely by using the magnetron sputtering system at Boston University, eliminating errors in device fabrication. Novel device designs similar to those described in ref.[85] can also be used to overcome the problems associated with the sapphire-gold interface and increase the reflectivity of the devices. Finally, the guidelines developed in the previous work for optimizing semiconductor-doped silica films for a given laser system can be used to select a different semiconductor material optimized for Ti:sapphire mode-locking. We expect that by combining the knowledge gained from our characterization of the linear and nonlinear optical properties of semiconductor-doped silica films with novel device designs and improved fabrication techniques, reflective semiconductor-doped silica film saturable absorbers can be developed and applied to self-starting mode-locking in solid-state lasers. This would be a major advance in ultrafast solid-state laser technology, enabling many applications that require inexpensive, compact ultrafast laser systems.

Femtosecond Nonlinear Material Processing

Femtosecond nonlinear materials processing is a powerful and versatile technique for fabricating photonic devices. Waveguides can be fabricated directly inside transparent materials by using a focused laser beam of femtosecond pulses. This technique promises to enable high-density photonic devices, since multiple layers of waveguides can be fabricated on a single substrate. Three-dimensional geometries, where waveguides interact in multiple dimensions, open the door to a wide range of new devices. Fabrication techniques are extremely versatile because devices are written simply by scanning the incident laser beam or the substrate. Thus, a wide range of different devices can be immediately fabricated under computer control. Devices can be designed, fabricated, and tested rapidly, streamlining the device development process.

The ability to produce structures inside materials requires the use of fabrication techniques that are mediated by nonlinear interaction of the laser pulses with the material. Therefore, nonlinear materials processing requires high-intensity pulses. Initial studies in this area relied on the use of laser amplifier systems in order to produce enough intensity to initiate the absorption process. [86] While this method does allow for processing of transparent materials, the speed and versatility is limited due to the low repetition rate of the laser systems in the kHz range. Because the interpulse arrival time exceeds the relaxation time of the material, structures are the result of the accumulation of many single shot interactions. For this reason, this fabrication method requires either very slow scanning, on the order of several tens of microns per second, or repeated scans of higher speed over the same area.

Recently, processing of transparent materials by using high-repetition-rate femtosecond oscillators has been reported. [87] In these studies, pulse energies of only ~10 nJ were used in conjunction with very tight focusing (~1.4 NA) to produce permanent structural changes in glass. Because of the high pulse repetition rate available from laser oscillators (MHz), the modification process is a multiple shot effect. Cumulative heating results from many pulses being deposited inside the focal volume at a rate faster than the material relaxation time. In addition to reducing the cost and complexity of the laser system, this method of material modification means that waveguides can be written at speeds that are significantly faster (~10 mm/s) than would possible with femtosecond amplifiers. Fabrication using laser oscillators has the additional advantage that scan speed can be modified to further optimize the exposure parameters.

During the previous contract period, our group developed a high-pulse energy, high-repetition-rate laser for femtosecond material processing using a multiple-pass cavity (MPC). Using prisms for dispersion compensation and a saturable-Bragg reflector (SBR) to stabilize pulses, our first generation multiple-pass cavity (MPC) laser generated maximum pulse energies of 90 nJ [88]. This increased performance enabled devices to be fabricated with less restrictive focusing at ~ 0.6 NA and was sufficient for many of our preliminary studies. Since then, we have developed a second generation MPC that eliminates the need for intracavity prisms by using double-chirped mirrors (DCM) for dispersion compensation [89]. The laser achieves significantly higher pulse energies, 150 nJ pulses at a repetition rate 50% higher than before (6 MHz vs. 4 MHz) with approximately 50% shorter pulse durations (43 fs vs. 80 fs) and peak powers up to 3.5 MW. Laser stability has also been significantly improved. This advance promises to lead to more reproducible fabrication with enhanced freedom to explore additional materials such as crystalline solids.

Waveguide fabrication and characterization

The characterization of the laser-induced changes in the material as well as waveguide device performance is a critical element of photonic device fabrication. In our initial investigation of waveguide fabrication we characterized the waveguide size as well as index change with respect to scan speed [90. Figure 44(a) shows a phase contrast image of waveguides fabricated at several scan speeds using an

effective 0.6 NA. There is a clear correlation between the diameter of the structure and the writing speed. Figure 44 (b) shows the transition from single-mode operation to higher-order modes as the waveguide size increases.

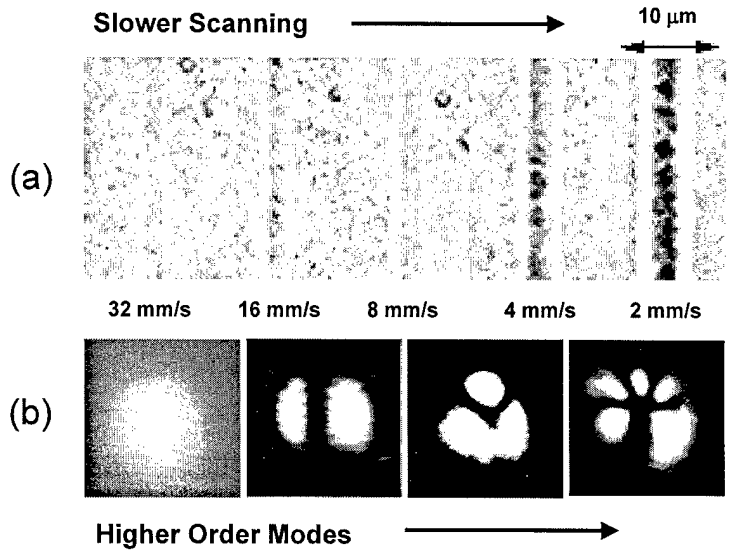

Figure 44. (a) Microscope image of fabricated waveguides at various scanning speeds, (b) output CCD image of waveguides showing transition from single-mode to higher order modes as scan speed is decreased (first images is for ~10 mm/s scanning)

As a compliment to waveguide size and mode dependence, we further characterized fabricated structures with Optical Coherence Tomography (OCT). OCT used low coherence interferometry to generate cross sectional images of backscattered or back-reflected light with high resolution and sensitivity. Because OCT has sensitivity to reflected signals as small as 10^{-10} of the incident beam as well as a high dynamic range, very accurate measurements of even a very small index change is possible. Figure 45 (a) shows a schematic representation of OCT imaging with the incident light reflecting from the top and bottom surface of the waveguide. The high longitudinal resolution (> 2 μm) of OCT enables the top and bottom of waveguide structures to be resolved. Figure 45 (b) shows the log signal with the peaks from the index difference at the waveguide interface separated by 4.6 μm from a representative waveguide, with the tomographic reconstructed image shown in (c). Figure 45 (d) shows the comparison with an end view from a phase-contrast microscope image.

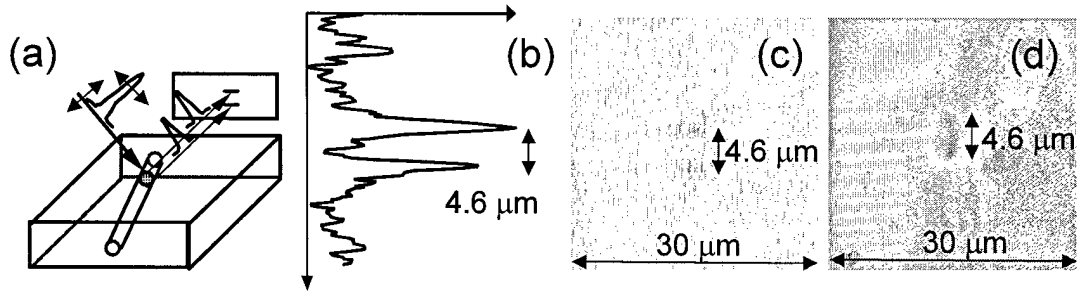

Figure 45. (a) Schematic representation of OCT imaging with light reflecting from the top and bottom surface of the waveguide, (b) log-demodulated signal showing peaks at the waveguide interfaces, (c) reconstructed tomographic OCT image compared to (d) end on view from a phase-contrast microscope.

In our future work, we plan to continue the investigation of waveguide fabrication in glass materials. While fabrication is often done with extremely tight focusing in order to get the modest pulse energy from standard oscillators to high enough intensity, our high-energy MPC allows this constraint to be relaxed. By varying the numerical aperture, scanning speeds, and exposures, we will examine the threshold for high-repetition-rate micro-machining. We will further characterize the waveguides fabricated under different parameters by examining waveguide size, index of refraction changes, and waveguiding properties.

Since waveguides are the building blocks of functional photonic devices, it is essential to conduct a comprehensive characterization of the waveguide structure and performance. To date we have been able to measure the index differential at the interface of our fabricated structure and the surrounding glass. While this is an important first step, a more in-depth study is necessary to fully characterize the index profile.

As a further study of fundamental structural changes in transparent materials, we plan to complete a two-color fabrication study. While fabrication studies at high-repetition rate have been performed [91] at UV wavelengths generated by nonlinear frequency conversion, data has been limited due to low pulse energies available in the UV wavelength regimes. Because our MPC laser can generate high-energy pulses, it will be possible to perform high-efficiency second-harmonic generation to obtain wavelengths in the 400 nm region. Comparing fabrication thresholds and material effects generated by IR versus UV pulses will provide important insight into the underlying nonlinear processes that produce the structural modifications. In addition, fabrication at shorter wavelengths should enable the fabrication of smaller structures than possible using IR pulses.

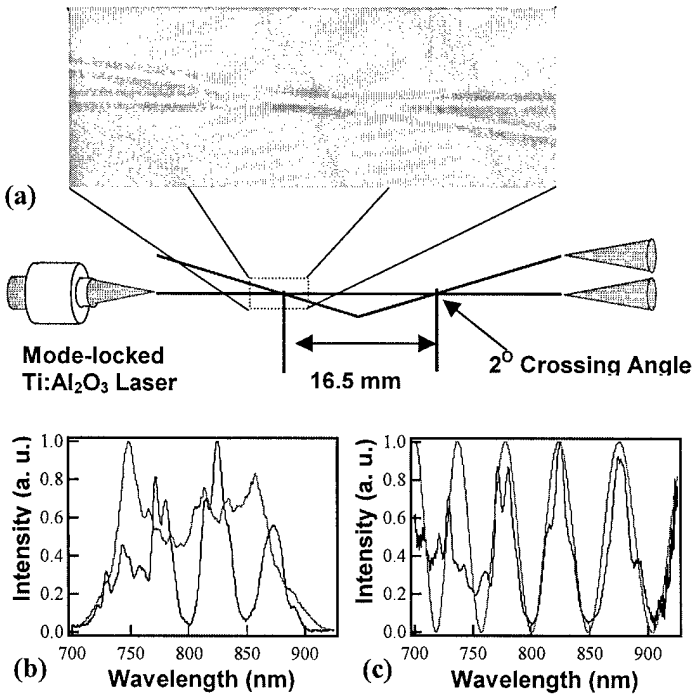

Figure 46. (a) Schematic of Mach-Zehnder interferometer with phase contrast image of x-coupler, (b) Input spectrum (gray) and output spectrum (gray) and, (c) normalized output spectrum (black) with sinusoidal fit for path length difference of 9.3 um.

Photonic device fabrication in glass

We have demonstrated the fabrication of several photonic device structures including x-couplers, and coupled mode devices. As an example of a more complex and usable device we have fabricated a Mach-Zehnder interferometer. [92] Interferometers are important in practical devices such as sensors and switches. Figure 46 (a) shows a schematic for the interferometer consisting of two back-to-back x-couplers with arms that differ in designed length by 10 μm. An interferometer with unbalanced arms acts as a wavelength dependant filter. When broadband radiation from a mode-locked laser is coupled into the interferometer (Figure 46 (b)), the normalized output (Figure 46(c)) shows a full modulation of the spectrum due to interference effects between the two arms.

Wavelength selective devices such as filters and resonators require complex structures. These devices are essential in WDM optical communication systems. In the fabrication techniques of such devices, not only simple linear waveguides, but also two- or three-dimensional structures, such as a rings or combinations of rings, are required. With the use of a computer controlled elliptically interpolating 3-D positioning system, we will be able to fabricate structures with high precision, uniformity, and reproducibility.

It will be possible to fabricate and characterize a wide range of new devices that depend on three-dimensional structures that cannot be built using standard techniques. We have previously demonstrated the ability to fabricate 3-D waveguides. [90] The fact that material interaction is mediated by nonlinear effects without linear absorption means that devices can be fabricated either above or below existing structures without producing collateral damage effects. Figure 47 (a) shows a cross sectional view of 3-D waveguides with mode coupling between adjacent guides shown in part (b). Figure 47 (c) shows a

schematic representation of several layered devices written one below the other in the same bulk material. By exploiting the 3rd dimension, a higher device density is achievable with the promise of increased functionality and greater compactness.

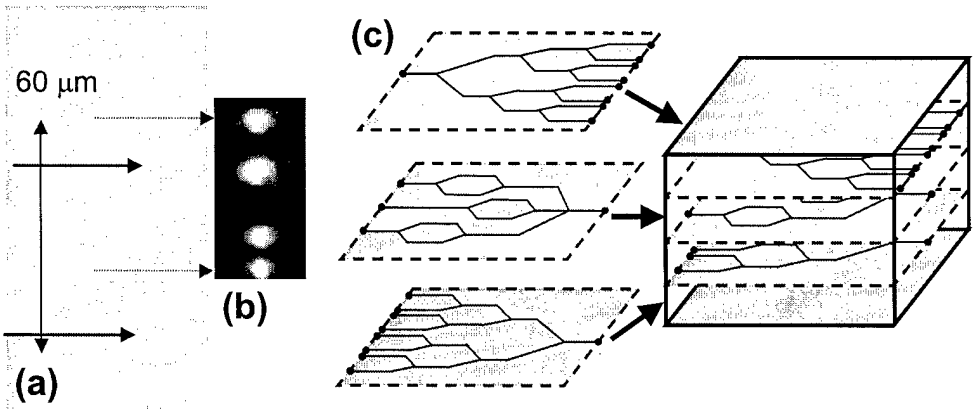

Figure 47. (a) Phase contrast image of layered waveguide structures. (b) CCD view of mode coupling between adjacent guides, and (c) schematic of layered photonic devices that are possible high-repetition rate femtosecond nonlinear material processing.

Micro-machining in other materials

Nonlinear material processing by femtosecond laser irradiation is not limited to glasses. The multi-photon nature of this fabrication technique can produce micron scale changes in wide variety of materials. We propose to investigate fabrication techniques in several different types of materials, such as doped glasses, semiconductors, and crystals.

The opportunity to integrate fabrication across several material choices promises to enable the development of novel devices such as active waveguides. Recently, optical amplification through waveguides fabricated in glass laser materials using femtosecond laser processing has been reported. [93] We will explore techniques for waveguide fabrication in laser gain media, and investigate their fluorescence and amplification performance. Efficient optical emission localized in a single-mode waveguide will be a promising light source as a high intensity illuminator, useful for a variety of applications including biomedical imaging. Moreover, by the integration of photonic devices such as gratings, amplifiers, and filters, a compact laser could be achieved.

We will explore approaches for fabricating waveguides in crystalline materials. This is especially challenging since it is necessary to preserve the crystalline order in the waveguide region. A variety of techniques such as treating regions adjacent to the waveguide to produce lower index amorphous regions will be investigated. If successful this fabrication technique would permit the development of waveguide lasers in a wide range of solid state materials. This fabrication technique would also have applications for nonlinear frequency conversion in nonlinear crystals.

References

[1] D. J. Jones, S. A. Diddams, J. K. Ranka, A. Stentz, R. S. Windeler, J. L. Hall, and S. T. Cundiff, "Carrier-Envelope Phase Control of Femtosecond Modelocked Lasers and Direct Optical Frequency Synthesis," *Science*, vol. 288, pp. 635-639, 2000.

[2] J. Zhou, G. Taft, C. P. Huang, M. M. Murnane, H. C. Kapteyn, and I. P. Christof, "Pulse evolution in a broad-bandwidth Ti:sapphire laser," *Optics Letters*, vol. 19, pp. 1149-1151, 1994.

[3] R. Szipöcs, K. Ferencz, C. Spielmann, and F. Krausz, "Chirped multilayer coatings for broadband dispersion control in femtosecond lasers," *Optics Letters*, vol. 19, pp. 201-203, 1994.

[4] R. Szipöcs and A. Kohazi-Kis, "Theory and design of chirped dielectric laser mirrors," *Applied Physics B*, vol. 65, pp. 115-136, 1997.

[5] N. Matuschek, F. X. Kärtner, and U. Keller, "Exact coupled-mode theories for multi-layer interference coatings with arbitrary strong index modulations," *IEEE Journal of Quantum Electronics*, vol. 33, pp. 295-302, 1997.

[6] F. X. Kärtner, N. Matuschek, T. Schibli, U. Keller, H. A. Haus, C. Heine, R. Morf, V. Scheuer, M. Tilsch, and T. Tschudi, "Design and fabrication of double-chirped mirrors," *Optics Letters*, vol. 22, pp. 831-833, 1997.

[7] N. Matuschek, "Theory and design of double-chirped mirrors.." Zurich: Swiss Federal Institute of Technology, 1999.

[8] R. Ell, U. Morgner, F. X. Kärtner, J. G. Fujimoto, E. P. Ippen, V. Scheuer, G. Angelow, and T. Tschudi, "Generation of 5 fs pulses and octave-spanning spectra directly from a Ti:sapphire laser," *Optics Letters*, vol. 26, pp. 373-375, 2001.

[9] A. Baltuska, A. Pugzlys, M. Pshenichnikov, D. Wiersma, B. Hoenders, and H. Ferwerda, "How to retrieve amplitude and phase from an autocorrelation and spectrum," presented at Proceedings of Ultrafast Optics, Ascona, Switzerland, 1999.

[10] F. X. Kärtner, U. Morgner, T. Schibli, E. P. Ippen, J. G. Fujimoto, V. Scheuer, G. Angelow, and T. Tschudi, "Ultrabroadband double-chirped mirror pairs for generation of octave spectra," *Journal of the Optical Society of America B*, vol. 18, pp. 882-885, 2001.

[11] A. M. Kowalevicz and et al., "Ultralow-threshold Kerr-lens mode-locked TiAl2O3 laser," *Optics Letters*, vol. 27, pp. 2037-2039, 2002.

[12] Y. P. Tong, P. M. W. French, J. R. Taylor, and J. G. Fujimoto, "All-solid-state femtosecond sources in the near infrared," *Optics Communications*, vol. 136, pp. 235-238, 1997.

[13] T. Tomaru and H. Petek, "Effect of third-order dispersion on the phases of solitonlike Cr4+:YAG-laser pulses characterized by the second-harmonic generation frequency resolved optical gating method," *Journal of the Optical Society of America B*, vol. 18, pp. 388-393, 2001.

[14] D. J. Ripin, C. Chudoba, J. T. Gopinath, J. G. Fujimoto, E. P. Ippen, U. Morgner, F. X. Kärtner, V. Scheuer, G. Angelow, and T. Tschudi, "Generation of 20-fs pulses by a prismless Cr4+:YAG laser," *Optics Letters*, vol. 27, pp. 61-63, 2002.

[15] D.J. Ripin, J.T. Gopinath, H.M. Shen, A.A. Erchak, G.S. Petrich, L.A. Kolodziejski, F.X. Kärtner and E.P. Ippen, "Oxidized GaAs/AlAs Mirror with a Quantum-Well Saturable Absorber for Ultrashort-Pulse Cr^{4+}:YAG Laser," Optics Communicaitons, 214, pp. 285-289, 2002

[16] C. Chudoba, J. G. Fujimoto, E. P. Ippen, H. A. Haus, U. Morgner, F. X. Kärtner, V. Scheuer, G. Angelow, and T. Tschudi, "All-solid-state Cr:forsterite laser generating 14 fs pulses at 1.3 μm," *Optics Letters*, vol. 26, pp. 292-294, 2001.

[17] I. Thomann and e. al., "A 420 MHz Cr:forsterite femtosecond ring laser and its use for continuum generation in the 1-2 micron range," presented at Conference on Lasers and Electro-Optics, Baltimore, USA, 2003.

[18] D. R. Herriot, H. Kogelnik, and R. Kompfner, "Off-axis paths in spherical mirror interferometers," *Applied Optics*, vol. 3, pp. 523-526, 1964.

[19] D. R. Herriot and H. J. Schulte, "Folded optical delay lines," *Applied Optics*, vol. 4, pp. 883-889, 1965.

[20] W. R. Trutna and R. L. Byer, "Multiple-pass Raman gain cell," *Applied Optics*, vol. 19, pp. 301-302, 1980.
[21] B. Perry, R. O. Brickman, A. Stein, E. B. Treacy, and P. Rabinowitz, "Controllable pulse compression in a multiple-pass-cell Raman laser," *Optics Communications*, vol. 34, pp. 3336-3348, 1980.
[22] J. B. McManus, P. L. Kebabia, and M. S. Zahniser, "Astigmatic mirror multipass absorption cells for long-path-length spectroscopy," *Optics Letters*, vol. 34, pp. 3336-3348, 1995.
[23] P. L. Hsiung, X. Li, C. Chudoba, I. Hartl, T. H. Ko, and J. G. Fujimoto, "High-speed path-length scanning with a multiple-pass cavity delay line," *Applied Optics*, vol. 42, pp. 640-648, 2003.
[24] A. R. Libertun, R. Shelton, H. C. Kapteyn, and M. M. Murnane, "A 36 nJ-15.5 MHz extended-cavity Ti:sapphire oscillator," presented at Conference on Lasers and Electro-Optics Technical Digest, 1999.
[25] S. H. Cho, B. E. Bouma, E. P. Ippen, and J. G. Fujimoto, "Low-repetition-rate high-peak-power Kerr-lens mode-locked Ti:Al2O3 laser with multi-pass cavity," *Optics Letters*, vol. 24, pp. 417-419, 1999.
[26] S. H. Cho, F. X. Kärtner, U. Morgner, E. P. Ippen, J. G. Fujimoto, J. E. Cunningham, and W. H. Knox, "Generation of 90-nJ pulses with a 4-MHz repetition-rate Kerr-lens mode-locked Ti:Al2O3 laser operating with net positive and negative intracavity dispersion," *Optics Letters*, vol. 26, pp. 560-562, 2001.
[27] A. Sennaroglu and J. G. Fujimoto, "Design criteria for Herriott-type multi-pass cavities for ultrashort pulse lasers," *Optics Express*, vol. 11, pp. 1106-1113, 2003.
[28] A. Sennaroglu, A. M. Kowalevicz, F. X. Kaertner, and J. G. Fujimoto, "High performance, compact, prismless, low-threshold 30 MHz Ti:Al2O3 laser," *Optics Letters*, in press.
[29] N. Matuschek, F. X. Kärtner, and U. Keller, "Analytic design of double-chirped mirrors with custom-tailored dispersion characteristics," *IEEE Journal of Quantum Electronics*, vol. 35, pp. 129-137, 1999.
[30] A. M. Kowalevicz, A. T. Zare, F. X. Kaertner, J. G. Fujimoto, S. Dewald, U. Morgner, V. Scheuer, and G. Angelow, "Generation of 150-nJ pulses from a multiple-pass cavity Kerr-lens modelocked Ti:Al2O3 oscillator," *Optics Letters*, in press.
[31] B. Agate, B. Stormont, A. J. Kemp, C. T. A. Brown, U. Keller, and W. Sibbett, "Simplified cavity designs for efficient and compact femtosecond Cr:LiSAF lasers," *Opt. Comm.*, vol. 205, pp. 207-213, 2002.
[32] J.-M. Hopkins, G. J. Valentine, B. Agate, A. J. Kemp, U. Keller, and W. Sibbett, "Highly compact and efficient femtosecond Cr:LiSAF lasers," *IEEE J. Quant. Elect.*, vol. 38, pp. 360-368, 2002.
[33] R. P. Prasankumar, Y. Hirakawa, A. M. Kowalevicz Jr., F. X. Kaertner, J. G. Fujimoto, and W. H. Knox, "An extended cavity femtosecond Cr:LiSAF laser pumped by low cost diode lasers," *Optics Express*, vol. 11, pp. 1265-1269, 2003.
[34] S. Tsuda, W. H. Knox, S. T. Cundiff, W. Y. Jan, and J. E. Cunningham, "Mode-locking ultrafast solid-state lasers with saturable Bragg reflectors," *IEEE J. Sel. Top. Quant. Elect.*, vol. 2, pp. 454-464, 1996.
[35] N. P. Ernsting and M. Kasche, "A reliable pump-probe, broadband spectrometer for subpicosecond transient absorption," *Review of Scientific Instruments*, vol. 62, pp. 600, 1991.
[36] I. Hartl, X. D. Li, S. H. Cho, R. K. Ghanta, T. H. Ko, J. G. Fujimoto, J. K. Ranka, and R. S. Windeler, "Ultrahigh-resolution optical coherence tomography using continuum generation in an air-silica microstructure optical fiber," *Optics Letters*, vol. 26, pp. 608, 2001.
[37] A. Baltuska, Z. Wei, M. Pshenichnikov, D. Wiersma, and R. Szipöcs, "All-solid-state cavity-dumped sub-5-fs laser," *Applied Physics B*, vol. 65, pp. 175-188, 1997.
[38] J. K. Ranka, R. S. Windeler, and A. Stentz, "Visible continuum generation in air-silica microstructure fibers with anomalous dispersion at 800 nm," *Optics Letters*, vol. 25, pp. 25, 2000.

[39] T. A. Birks, W. J. Wadsworth, and P. S. J. Russell, "Supercontinuum generation in tapered fibers," *Optics Letters*, vol. 25, pp. 1415, 2000.

[40] M. Nisoli, S. De Silvestri, O. Svelto, K. Ferencz, C. Spielmann, S. Sartania, and F. Krausz, "Compression of high-energy laser pulses below 5 fs," *Optics Letters*, vol. 22, pp. 522, 1997.

[41] P. Poirier and F. Hanson, "Intracavity frequency doubling of a 2.5-kHz pulsed Ti:Al2O3 laser," *Optics Letters*, vol. 18, pp. 1925-1927, 1993.

[42] A. M. Weiner, A. M. Kan'an, and D. E. Leaird, "High-efficiency blue generation by frequency doubling of femtosecond pulses in a thick nonlinear crystal," *Optics Letters*, vol. 23, pp. 1441-1443, 1998.

[43] D. Steinbach, W. Hugel, and M. Wegener, "Generation and detection of blue 10.0-fs pulses," *Journal of the Optical Society of America B*, vol. 15, pp. 1231-1234, 1998.

[44] F. Rotermund and V. Petrov, "Generation of the fourth harmonic of a femtosecond Ti:sapphire laser," *Optics Letters*, vol. 23, pp. 1040-1042, 1998.

[45] M. Pierrou, F. Laurell, H. Karlsson, T. Kellner, C. Czeranowsky, and G. Huber, "Generation of 740 nW of blue light by intracavity frequency doubling with first-order quasi-phase-matched $KTiOPO_4$ crystal," *Optics Letters*, vol. 24, pp. 205-207, 1999.

[46] C. G. Durfee III, S. Backus, H. C. Kapteyn, and M. M. Murnane, "Intense 8-fs pulse generation in the deep ultraviolet," *Optics Letters*, vol. 24, pp. 697-699, 1999.

[47] S. Yu and A. M. Weiner, "Phase-matching temperature shifts in blue generation by frequency doubling of femtosecond pulses in $KNbO_3$," *Journal of the Optical Society of America B*, vol. 16, pp. 1300-1304, 1999.

[48] B. Agate, A. J. Kemp, C. T. A. Brown, and W. Sibbett, "Efficient, high-repetition-rate femtosecond blue source using a compact Cr:LiSAF laser," *Optics Express*, vol. 10, pp. 824-831, 2002.

[49] M. Ramaswamy, M. Ulman, J. Paye, and J. G. Fujimoto, "Cavity-dumped femtosecond Kerr-lens modelocked Ti:Al2O3 laser," *Optics Letters*, vol. 18, pp. 1822, 1993.

[50] M. Pshenichnikov, W. P. de Boeij, and D. Wiersma, "Generation of 13-fs, 5-MW pulses from a cavity-dumped Ti:sapphire laser," *Optics Letters*, vol. 19, pp. 572, 1994.

[51] H. A. Haus, E. P. Ippen, and J. G. Fujimoto, "Structures for additive pulse modelocking," *Journal of the Optical Society of America B*, vol. 16, pp. 1502-04, 1991.

[52] P. A. Schulz and S. R. Henion, "Liquid-Nitrogen-Cooled Ti:Al2O3 Laser," *IEEE Journal of Quantum Electronics*, vol. 27, pp. 1039-1047, 1991.

[53] M. Zavelani-Rossi, F. Linder, C. Le Blanc, G. Cheriaux, and J. P. Chambaret, "Control of thermal effects for high-intensity Ti:sapphire laser chains," *Applied Physics B*, vol. 70[Suppl.], pp. S193-S196, 2000.

[54] L. A. Jiang, M. E. Grein, E. P. Ippen, C. McNeilage, J. Searls and H. Yokoyama, "Quantum-limited Noise Performance of a Mode-locked Laser Diode," *Optics Letters*, 27, 49 (2002)

[55] D.J Jones, K.W. Holman, M. Notcutt, J. Ye, J. Chandalia, L.A. Jiang, E. P. Ippen and H. Yokoyama, "Ultralow-jitter, 1550-nm Mode-locked Semiconductor Laser Synchronized to a Visible Optical Frequency Standard," *Optics Letters*, 28, 313 (2003)

[56] F. Rana, H.l.T. Lee, R. Ram, M. E. Grein, L. A. Jiang, E. P. Ippen and H. A. Haus, "Characterization of the Noise and Correlations in Harmonically Mode-Locked Lasers," *JOSA B* 19, 2609 (2002)

[57] T. R. Schibli, T. Kremp, U. Morgner, F.X. Kärtner, R. Butendeich, J. Schwarz, H. Schweizer and F. Scholz, "CW-operation and Q-switched mode locking of Cr:YAG-microchip lasers," Optics Letters, 26, 48 (2001)

[58] T. R. Schibli, U. Morgner and F.X. Kärtner, "Control of Q-switched mode locking by active feedback," Optics Letters, 26, 148 (2001)

[59] T. R. Schibli, U. Morgner and F.X. Kärtner, PCT Patent application. 2001

[60] M. E. Grein, L. A. Jiang, Y. Chen, H A. Haus, and E. P. Ippen, Ippen, "Timing Restoration Dynamics in an Actively Mode-Locked Fiber Ring Laser," *Optics Letters*, 24 1687 (1999)

[61] M. E. Grein, L. A. Jiang, H. A. Haus, and E. P. Ippen, C. McNeilage, J. H. Searls, and R. S. Windeler, *Optics Letters*, 27, 957 (2002)
[62] T. P. Carruthers and I. N. Duling III, *Optics Letters*, 21, 1927 (1996)
[63] H. Sotobayashi, J. Gopinath and E. P. Ippen, to be published in Electronics Letters
[64] T. R. Schibli, E. R. Thoen, F. X. Kaertner and E. P. Ippen, "Suppression of Q-switched mode locking and break-up into multiple pulses by inverse saturable absorption," *Applied Physics B*, B70: S41-S49 (2000)
[65] J. D. Kafka, M. L. Watts and J. W. Pieterse, "Synchronously pumped optical parametric oscillators with LiB3O5," *JOSA B*, 12(11): 2147-2157 (1995)
[66] K. S. Abedin, J. T. Gopinath, E. P. Ippen, C. E. Kerbage, R. S. Windeler and B. J. Eggleton, "Highly non-degenerate femtosecond four-wave mixing in tapered fiber," *Applied Physics Letters*, 81, 1384 (2002)
[67] K. L. Hall, E. R. Thoen and E. P. Ippen,, "Nonlinearities in Active Media," *Semiconductors and Semimetals*, Chapter 2, Vol 59, Eds. E. Garmire and A. Kost, Academic Press, 1998
[68] B. S. Robinson, S. A. Hamilton and E. P. Ippen, "Multiple wavelength demultiplexing using an ultrafast nonlinear interfermeter," *Tech. Digest, CLEO'01*, Optical Society of America, 2001
[69] M. Ibanescu, S. G. Johnson, M Soljacic, J. D. Joannopoulos and Y. Fink, Physical Review E, 67, 046601-1 (2003)
[70] S. Hughes, "Breakdown of the Area Theorem: Carrier-Wave Rabi Flopping of Femtosecond Optical Pulses," *Physical Review Letters,* 81, 3363 (1998)
[71] O. D. Mücke, T. Tritschler, M. Wegener, U. Morgner and F.X. Kärtner, "Signatures of Carrier-Wave Rabi-Flopping in GaAs," *Physical Review Letters,* 87, 057401-1 (2001)
[72] O.D. Mücke, T. Tritschler, M. Wegener, U. Morgner, F.X. Kärtner, G. Khitrova and H.M. Gibbs, "The carrier-wave Mollow triplet and its dependence on the carrier-envelope offset phase," to appear in *Physical Review Letters*
[73] U. Keller, K. J. Weingarten, F. X. Kärtner, D. Kopf, B. Braun, I. D. Jung, R. Fluck, C. Hönninger, N. Matuschek, and J. Aus der Au, "Semiconductor saturable absorber mirrors (SESAMs) for femtosecond to nanosecond pulse generation in solid-state lasers," *IEEE J. Sel. Top. Quant. Elect. (JSTQE)*, vol. 2, pp. 435-453, 1996.
[74] I. D. Jung, F. X. Kärtner, N. Matuschek, D. H. Sutter, F. Morier-Genoud, Z. Shi, V. Scheuer, M. Tilsch, T. Tschudi, and U. Keller, "Semiconductor saturable absorber mirrors supporting sub-10 fs pulses," *Appl. Phys. B*, vol. 65, pp. 137-150, 1997.
[75] D. H. Sutter, G. Steinmeyer, L. Gallmann, N. Matuschek, F. Morier-Genoud, U. Keller, V. Scheuer, G. Angelow, and T. Tschudi, "Semiconductor saturable-absorber mirror assisted Kerr-lens mode-locked Ti:sapphire laser producing pulses in the two-cycle regime," *Opt. Lett.*, vol. 24, pp. 631-633, 1999.
[76] I. P. Bilinsky, J. G. Fujimoto, J. N. Walpole, and L. J. Misaggia, "Semiconductor-doped silica saturable absorber films for solid state laser mode locking," *Opt. Lett.*, vol. 23, pp. 1766-1768, 1998.
[77] K. Tsunetomo, H. Nasu, H. Kitayama, A. Kawabuchi, Y. Osaka, and K. Takiyama, "Quantum size effect of semiconductor microcrystallites doped in SiO2-glass thin films prepared by RF-sputtering," *Japanese Journal of Applied Physics*, vol. 28, pp. 1928-1933, 1989.
[78] K. Tsunetomo, M. Yamamoto, and Y. Osaka, "CuCl microcrystallite-doped SiO2 glass thin films prepared by RF sputtering," *Japanese Journal of Applied Physics*, vol. 30, pp. L764, 1991.
[79] S. Kaneko, H. Hasu, T. Ikegami, J. Matsuoka, and K. Kamiya, "Effect of preparation conditions on the properties of CdSe microcrystal-doped SiO2 glass thin films prepared by RF-sputtering," *Japanese Journal of Applied Physics*, vol. 30, pp. L764, 1992.
[80] I. P. Bilinsky, J. G. Fujimoto, J. N. Walpole, and L. J. Misaggia, "InAs-doped silica films for saturable absorber applications," *Appl. Phys. Lett.*, vol. 74, pp. 2411-2413, 1999.

[81] S. Kaneko, H. Nasu, T. Ikegami, J. Matsuoka, and K. Kamiya, "Effect of preparation conditions on the properties of CdSe microcrystal-doped SiO_2 glass thin films prepared by RF-sputtering," *Jap. J. Appl. Phys.*, vol. 31, pp. 2206-2211, 1992.

[82] I. Tanahashi, A. Tsujimura, T. Mitsuyu, and A. Nishino, "Optical properties of CdS microcrystallite-doped SiO_2 glass thin films," *Jap. J. Appl. Phys.*, vol. 29, pp. 2111-2115, 1990.

[83] R. P. Prasankumar, C. Chudoba, J. G. Fujimoto, P. Mak, and M. F. Ruane, "Self-starting mode locking in a Cr:forsterite laser by use of non-epitaxially-grown semiconductor-doped silica films," *Optics Letters*, vol. 27, pp. 1564-66, 2002.

[84] D. M. Mittleman, R. W. Schoenlein, J. J. Shiang, V. L. Colvin, A. P. Alivisatos, and C. V. Shank, "Quantum size dependence of femtosecond electronic dephasing and vibrational dynamics in CdSe nanocrystals," **Phys. Rev. B**, vol. 49, pp. 14435-14447, 1994.

[85] Z. Zhang, K. Torizuka, T. Itatani, K. Kobayashi, T. Sugaya, T. Nakagawa, and H. Takahashi, "Broadband semiconductor saturable-absorber mirror for a self-starting mode-locked Cr:forsterite laser," *Optics Letters*, vol. 23, pp. 1465-7, 1998.

[86] K. M. Davis, K. Miura, N. Sugimoto, and K. Hirao, "Writing waveguides in glass with a femtosecond laser," *Optics Letters*, vol. 21, pp. 1729-1731, 1996.

[87] C. B. Schaffer, A. Brodeur, J. F. Garcia, and E. Mazur, "Micromachining bulk glass by use of femtosecond laser pulses with nanojoule energy," *Optics Letters*, vol. 26, pp. 93, 2001.

[88] S. H. Cho, F. X. Kärtner, U. Morgner, E. P. Ippen, J. G. Fujimoto, J. E. Cunningham, and W. H. Knox, "High energy pulse generation using a 4 MHz repetition rate KLM Ti:Al2O3 laser operating with positive and negative dispersion," *Optics Letters*, vol. 26, pp. 560, 2001.

[89] A. M. Kowalevicz, A. T. Zare, F. X. Kaertner, J. G. Fujimoto, S. Dewald, U. Morgner, V. Scheuer, and G. Angelow, "Generation of 150-nJ pulses from a multiple-pass cavity Kerr-lens modelocked Ti:Al2O3 oscillator," to be published, *Optics Letters*, 2003.

[90] K. Minoshima, A. M. Kowalevicz, I. Hartl, E. P. Ippen, and J. G. Fujimoto, "Photonic device fabrication in glass by use of nonlinear materials processing with a femtosecond laser oscillator," *Optics Letters*, vol. 26, pp. 1516-1518, 2001.

[91] A. M. Streltsov and N. F. Borrelli, "Study of femtosecond-laser-written waveguides in glasses," *Journal of the Optical Society of America B Optical Physics*, vol. 19, pp. 2496-2504, 2002.

[92] K. Minoshima, A. M. Kowalevicz, E. P. Ippen, and J. G. Fujimoto, "Fabrication of coupled mode photonic devices in glass by nonlinear femtosecond laser materials processing," *Optics Express*, vol. 10, pp. 645-652, 2002.

[93] Y. Sikorski, A. A. Said, P. Bado, R. Maynard, C. Florea, and K. A. Winick, "Optical waveguide amplifier in Nd doped glass written with near-IR femtosecond laser pulses," *Electronic Letters*, vol. 36, 2000.

Publications acknowledging AFOSR Contract No. F49620-01-1-0084

1. U. Morgner, W. Drexler, F.X. Kärtner, X. D. Li, C. Pitris, E. P. Ippen, J. G. Fujimoto, "Spectroscopic optical coherence tomography," *Optics Letters* 25, 111-113, 2000.

2. J. G. Fujimoto, C. Pitris, S. Boppart, and M. Brezinski, "Optical coherence tomography, an emerging technology for biomedical imaging and optical biopsy," *Neoplasia* 2, 9-25, 2000.

3. T.R. Schibli, E.R. Thoen, F.X. Kärtner and E.P. Ippen, "Suppression of Q-switched Modelocking and Break-up into Multiple Pulses by Inverse Saturable Absorption, " *Applied Physics B.*, 70, S41-S49, 2000.

4. S.B. Fleischer, B. Pevzner, D.J. Dougherty, H.J. Zeiger, G. Dresselhaus, M.S. Dresselhaus, E.P. Ippen and A.F. Hebard, "Ultrafast Dynamics of Superconducting K_3C_{60} and Rb_3C_{60}," *Physical Review B*, 60, pp. 1366-1378, 2000.

5. E.R. Thoen, M.E. Grein, E.M. Koontz, E.P. Ippen, H.A. Haus and L.A. Kolodziejski, "Stabilization of an Active Harmonically Mode-locked Fiber Laser Using Two-photon Absorption, " *Optics Letters* 25, pp. 948-950, 2000.

6. C.X. Yu, H.A. Haus, E.P. Ippen, W.S. Wong and A. Sysoliatin, "Gigahertz-repetition-rate mode - locked fiber laser for continuum generation," *Optics Letters* 25, 1418-1420, 2000.

7. C. Chuboda, J.G. Fujimoto, E.P. Ippen, H.A. Haus, U. Morgner, F.X. Kärtner, V. Scheuer, G. Angelow and T. Tshudi, "14-fs Pulses at 1.3 mm Generated from an All-Solid-State Cr:forsterite Laser," Springer Series in Chem. Phys. 66, *Ultrafast Phenomena XII,* Springer Verlag, 59-61, 2001.

8. L.A. Jiang, M.E. Grein, H.A. Haus and E.P. Ippen, "Noise of Mode-Locked Semiconductor Lasers," *IEEE J. on Selected Topics in Quantum Electronics*, 7, 159-167, 2001.

9. R. Ell, U. Morgner, F.X. Kärtner, J.G. Fujimoto, E.P. Ippen, V. Scheuer, G. Angelow, T. Tschudi, M..J. Lederer, A. Boiko and B. Luther-Davies, "Generation of 5-fs Pulses and Octave-Spanning Spectra Directly from a Ti:Sapphire Laser," *Optics Letters*, 26, 373-375, 2001.

10. C. Chudoba, J. G. Fujimoto, E. P. Ippen, H. A. Haus, U. Morgner, F. X. Kartner, V. Scheuer, G. Angelow, and T. Tschudi, "All-solid-state Cr:forsterite laser generating 14 fs pulses at 1.3 μm," *Optics Letters* 26, 292-294, 2001.

11. R. Ell, U. Morgner, F. X. Kärtner, J. G. Fujimoto, E. P. Ippen, V. Scheuer, G. Angelow, T. Tschudi, M. J. Lederer, A. Boiko, and B. Luther-Davies, "Generation of 5-fs pulses and octave-spanning spectra directly from a Ti:Sapphire laser," *Optics Letters* 26, 373-375, 2001.

12. S. H. Cho, F. X. Kärtner, U. Morgner, E. P. Ippen and J. G. Fujimoto, "Generation of 90-nJ pulses with a 4-MHz repetition-rate Kerr-lens mode-locked $Ti:Al_2O_3$ laser operating with net positive and negative intracavity dispersion," *Optics Letters* 26, pp.560-562, 2001.

13. W. Drexler, U. Morgner, R. K. Ghanta, F. X. Kärtner, J. S. Schuman, J.G. Fujimoto, "Ultrahigh resolution ophthalmic optical coherence tomography," *Nature Medicine* 7, 502-507, 2001.

14. S. H. Cho, F. X. Kärtner, U. Morgner, E. P. Ippen, J. G. Fujimoto, J. E. Cunningham, W. H. Knox, "Generation of 90-nJ pulses with a 4 MHz repetition-rate Kerr-lens mode-locked Ti:Al_2O_3 laser operating with net positive and negative intracavity dispersion," *Optics Letters* 26, 560-562, 2001.

15. I. Hartl, X.D. Li, C. Chudoba, R. Ghanta, T. Ko, J.G. Fujimoto, J. K. Ranka, R. S. Windeler, and A. J. Stentz, "Ultrahigh resolution optical coherence tomography using continuum generation in an air-silica microstructure optical fiber," *Optics Letters* 26, 608-610, 2001.

16. C.X. Yu, H.A. Haus and E.P. Ippen, "Soliton Squeezing at the Gigahertz Rate in a Sagnac Loop," *Optics Letters* 26, 669-671, 2001.

17. J.T. Gopinath, E.R. Thoen, E.M. Koontz, M.E. Grein, L.A. Kolodziejski and E.P. Ippen, "Recovery Dynamics in Proton-Bombarded Semiconductor Saturable Absorber Mirrors," *Applied Physics Letters* 78, 3409-3411, 2001.

18. U. Morgner, R. Ell, G. Metzler, T. R. Schibli, J. G. Fujimoto, E. P. Ippen, and F. X. Kärtner, "Nonlinear optics with phase-controlled pulses in the sub-two-cycle regime," *Physical Review Letters* 86, 5462-5465, 2001.

19. F.X. Kärtner, U. Morgner, R. Ell, T. Schibli, J.G. Fujimoto, E.P. Ippen, V. Scheuer, G. Angelow and T. Tschudi, "Ultrabroadband Double-Chirped Mirror Pairs for Generation of Octave Spectra," *J. Optical Society of America B*, 18, 882-885, 2001.

20. K. Minoshima, A.M. Kowalevicz, I. Hartl, E. P. Ippen and J. G. Fujimoto, "Photonic Device Fabrication in Glass by Use of Nonlinear Materials Processing with a Femtosecond Laser Oscillator," *Optics Letters* 26, 1516-1518, 2001.

21. H. A. Haus and E. P. Ippen, "Group Velocity of Solitons," *Optics Letters* 26, 1654-1656, 2001.

22. D.J. Ripin, C. Chudoba, J.T. Gopinath, J.G. Fujimoto, E.P. Ippen, U. Morgner, F.X. Kärtner, V. Scheuer, G. Angelow and T. Tschudi, "Generation of 20-fs Pulses by a Prismless Cr^{4+}YAG Laser," *Optics Letters* 27, 61-63, 2002.

23. L.A. Jiang, M.E. Grein, E.P. Ippen, C. McNeilage, J. Searls, and H. Yokoyama, "Quantum-limited Noise Performance of a Mode-locked Laser Diode," *Optics Letters* 27, 49-51, 2002.

24. A. M. Kowalevicz, T. Ko, I. Hartl, J. G. Fujimoto, M. Pollnau, and R. P. Salathe, "Ultrahigh resolution optical coherence tomography using a superluminescent light source," *Optics Express* 10, 349-353, 2002.

25. K. Minoshima, A.M. Kowalevicz, E.P. Ippen and J.G. Fujimoto, "Fabrication of Coupled Mode Photonic Devices in Glass by Nonlinear Femtosecond Laser Materials Processing," *Optics Express*, 10, 645-652, 2002.

26. K.S. Abedin, J.T. Gopinath, E.P. Ippen, C.E. Kerbage, R.S. Windeler and B.J. Eggleton, "Highly Nondegenerate Femtosecond Four-wave Mixing in Tapered Microstructure Fiber," *Applied Physics Letters* 81, 1384-1386, 2002.

27. R. P. Prasankumar, C. Chudoba, J. G. Fujimoto, P. Mak, and M. F. Ruane, "Self-starting modelocking in a Cr:Forsterite laser by use of non-epitaxially-grown semiconductor-doped silica films," *Optics Letters* 27, 1564-1566, 2002.

28. D.J. Ripin, J.T. Gopinath, H.M. Shen, A.A. Erchak, G.S. Petrich, L.A. Kolodziejski, F.X. Kärtner and E.P. Ippen, "Oxidized GaAs/AlAs Mirror with a Quantum-Well Saturable Absorber for Ultrashort-Pulse Cr^{4+}:YAG Laser," *Optics Communications*, 214, 285-289, 2002.

29. K.S. Abedin, J.T. Gopinath, L.A. Jiang, M.E. Grein, H.A. Haus and E.P. Ippen, "Self-Stabilized Passive, Harmonically Mode-Locked Stretched-Pulse Erbium Fiber Ring Laser," *Optics Letters*, 27, 1758-1760, 2002.

30. A. M. Kowalevicz, T. R. Schibli, F. X. Kartner, and J. G. Fujimoto, "Ultra-low-threshold Kerr lens modelocked Ti:Al_2O_3 lasers," *Optics Letters* 27, 2037-2039, 2002.

31. L.A. Jiang, M.E. Grein, J.K. Chandalia, E.P. Ippen and H. Yokoyama, "Retiming Dynamics of Modelocked Semiconductor Laser," *Electronics Letters* 38, 1447-1447, 2002.

32. S. Demos, M. Staggs, K. Minoshima, J. Fujimoto, "Characterization of laser induced damage sites in optical components," *Optics Express* 10, 1444-1450, 2002.

33. S.A. Hamilton, B.S. Robinson, T.E. Murphy, S.J. Savage, and E.P. Ippen, "100 Gb/s Optical Time-Division Multiplexed Networks," *J. Lightwave Technology* 20, 1-15, 2002.

34. L.A. Jiang, M.E. Grein, H.A. Haus and E.P. Ippen, "Timing Jitter Eater for Optical Pulse Trains," *Optics Letters* 28, 78-80, 2003.

35. P. L. Hsiung, X. Li, C. Chudoba, I. Hartl, T. H. Ko, and J. G. Fujimoto, "High speed path length scanning using a Herriott cell delay line," *Applied Optics*, 42, 640-648, 2003.

36. D.J. Jones, K.W. Holman, M. Notcutt, J. Ye, J. Chandalia, L.A. Jiang and E.P. Ippen, "Ultralow-jitter, 1550-nm mode-locked semiconductor laser synchronized to a visible optical frequency standard," *Optics Letters* 28, 813-815, 2003.

37. T.R. Schibli, J. Kim, O. Kuzucu, J.T. Gopinath, S.N. Tandon, G.S. Petrich, L.A. Koldoziejski, J.G. Fujimoto, E.P. Ippen and F.X. Kaertner, "Attosecond active synchronization of passively mode-locked lasers by balanced cross correlation," *Optics Letters* 28, 947-949, 2003.

38. S. Bourquin, R. P. Prasankumar, F. X. Kaertner, J. G. Fujimoto, T. Lasser and R. P. Salathe, "High-speed femtosecond pump-probe spectroscopy with a smart pixel detector array," *Optics Letters* 28, 1588-1590, 2003.

39. A. M. Kowalevicz, Jr., A. Tucay Zare, F. X. Kaertner, J. G. Fujimoto, S. Dewald, U. Morgner, V. Scheuer and G. Angelow, "Generation of 150nJ pulses from a multiple-pass cavity Kerr-lens mode-locked Ti:Al_2O_3 oscillator," *Optics Letters* 28, 1597-1599, 2003.

40. D.J. Jones, K.W. Holman, M. Notcutt, J. Ye, J. Chandalia, L.A. Jiang and E.P. Ippen, "Ultralow-jitter, 1550-nm mode-locked semiconductor laser synchronized to a visible optical frequency standard," *Optics Letters* 28, 813-815, 2003.

41. T.R. Schibli, O. Kuzucu, J.W. Kim, E. P. Ippen, J. G. Fujimoto, F.X. Kaertner, V. Scheuer and G. Angelow, "Toward Single-Cycle Laser Systems," *IEEE J. Select. Topics in Quantum. Electron.* 9, 1-3, 2003.

42. H. Sotobayashi, J.T. Gopinath and E.P. Ippen, "23-cm-long Bi_2O_3-based EDFA for picosecond pulse amplification with 80 nm gain bandwidth," *Electron. Letters* 39, 1374-1375, 2003.

43. K.W. Holman, D.J. Jones, J. Ye, and E.P. Ippen, "Orthogonal Control of the Frequency Comb Dynamics of a Mode-Locked Laser Diode," *Optics Letters* 28, pp. 2405-2407, 2003.

44. J.T. Gopinath, H.Sotobayashi and E.P. Ippen, "Broadband Amplification of Picosecond Pulses in a 23 cm length of Bi_2O_3-based Erbium-doped Fiber," *OSA TOPS* 92, pp. 50-53, 2003.

45. K.W. Holman, D.J. Jones, S. Cundiff, J. Ye, J.B. Schlager and E.P. Ippen, "Optical Phase-Coherent Link Between an Optical Atomic Clock and 1550 nm Mode-Locked Lasers," *IEEE LEOS Newsletter*, pp. 6-8, December 2003.